nature aging

Article

https://doi.org/10.1038/s43587-023-00451-9

Multi-omic rejuvenation and lifespan extension on exposure to youthful circulation

Received: 23 November 2021

Accepted: 6 June 2023

Published online: 27 July 2023

Check for updates

Bohan Zhang[1,13], David E. Lee[2,3,13], Alexandre Trapp[1,9,13], Alexander Tyshkovskiy[1,4], Ake T. Lu[5,10], Akshay Bareja[2,3], Csaba Kerepesi[1,11], Lauren K. McKay[3,12], Anastasia V. Shindyapina[1,9], Sergey E. Dmitriev[4], Gurpreet S. Baht[3,6,7], Steve Horvath[5,8,10], Vadim N. Gladyshev[1] ✉ & James P. White[2,3,7] ✉

Heterochronic parabiosis (HPB) is known for its functional rejuvenation effects across several mouse tissues. However, its impact on biological age and long-term health is unknown. Here we performed extended (3-month) HPB, followed by a 2-month detachment period of anastomosed pairs. Old detached mice exhibited improved physiological parameters and lived longer than control isochronic mice. HPB drastically reduced the epigenetic age of blood and liver based on several clock models using two independent platforms. Remarkably, this rejuvenation effect persisted even after 2 months of detachment. Transcriptomic and epigenomic profiles of anastomosed mice showed an intermediate phenotype between old and young, suggesting a global multi-omic rejuvenation effect. In addition, old HPB mice showed gene expression changes opposite to aging but akin to several lifespan-extending interventions. Altogether, we reveal that long-term HPB results in lasting epigenetic and transcriptome remodeling, culminating in the extension of lifespan and healthspan.

Aging is the primary risk factor for chronic diseases[1–3]. It brings accumulation of damage at many levels of biological organization and a pervasive and destructive decline of organ function, resulting in inevitable mortality. Although many attempts have been made to extend the lifespan and ameliorate specific aging phenotypes through interventions, aging itself has generally been regarded as an irreversible process. However, the recent development and application of advanced aging biomarkers based on DNA methylation (that is, methylation clocks)[4–7] have challenged this concept. With their assessment of the attenuated aging effect of various longevity interventions, including caloric restriction (CR), genetic models and cellular reprogramming, methylation clocks have been generally recognized as a robust predictor of organismal biological age, a measure of how old an organism is biologically rather than chronologically. Notably, DNA methylation

[1]Division of Genetics, Department of Medicine, Brigham and Women's Hospital, Harvard Medical School, Boston, MA, USA. [2]Department of Medicine, Duke University School of Medicine, Durham, NC, USA. [3]Duke Molecular Physiology Institute, Duke University, Durham, NC, USA. [4]Belozersky Institute of Physico-Chemical Biology, Moscow State University, Moscow, Russia. [5]Department of Human Genetics, David Geffen School of Medicine, University of California, Los Angeles, CA, USA. [6]Department of Orthopaedic Surgery, Duke University School of Medicine, Durham, NC, USA. [7]Duke Center for the Study of Aging and Human Development, Duke University School of Medicine, Durham, NC, USA. [8]Department of Biostatistics, School of Public Health, University of California, Los Angeles, CA, USA. [9]Present address: Retro Biosciences, Redwood City, CA, USA. [10]Present address: Altos Labs, San Diego, CA, USA. [11]Present address: Institute for Computer Science and Control (SZTAKI), Eötvös Loránd Research Network, Budapest, Hungary. [12]Present address: Division of Oral and Craniofacial Health Sciences, Adams School of Dentistry, University of North Carolina at Chapel Hill, Chapel Hill, NC, USA. [13]These authors contributed equally: Bohan Zhang, David E. Lee, Alexandre Trapp. ✉e-mail: vgladyshev@rics.bwh.harvard.edu; james.white@duke.edu

clocks have successfully predicted the reversal of epigenetic age by several interventions, including reprogramming factor expression and treatment with drugs or blood components[8–12]. Recently, clocks have also been used to reveal and describe a natural rejuvenation event occurring during early embryonic development[13,14]. However, in the case of interventions, it is generally enigmatic whether the predicted reversal of epigenetic age is sustained, correlated with longer lifespan and manifests in improved physiological function.

Since the 1950s, the heterochronic parabiosis (HPB) model has been used to study circulating factors that regulate the aging process[15–17]. More recent work has established this model as a proof of concept that youthful circulation can restore old tissue functions[18,19]. Indeed, the effects of HPB on the amelioration of aging phenotypes are evident across tissues including muscle[19], liver[19], heart[20], brain[21,22] and bone[18,23]. Remarkably, these effects are observed typically after only 4–5 weeks of parabiosis. Similar results are observed with acute heterochronic blood exchange (non-parabiosis), showing beneficial effects of 'young blood' on the muscle, liver and brain of old recipients[24]. Heterochronic young blood plasma transfer also improves pathology of age-related diseases, as in a model of Alzheimer's disease in mice[25]. Although HPB leads to diverse effects on old cells and tissues, our understanding of the molecular mechanisms involved is limited. Likewise, whether the immediate effects of blood and plasma exchange are sustained after the procedure is still unknown. Lastly, due to the previous absence of a precise quantification method, it is unclear whether HPB can slow or rewind the epigenetic aging of an organism.

A previously reported[26,27] but seldom used HPB procedure is the detachment of mice after parabiosis. This technique has previously been used to verify cell engraftment using different tracer techniques[28]. A recent investigation revealed the persistence of aged hematopoietic stem cells in the young bone marrow niche resulting from HPB months after surgical separation of parabionts[29]; however, to our knowledge, there have been no studies that investigate longevity or the long-term effects of HPB on healthspan. Although detachment involves performing a second surgery on the animals, it permits physiological and longevity measurements that are difficult to obtain in the case of anastomosed mice.

In this study, we report the results of a long-term HPB study followed by a detachment period. We found that old mice detached from young mice showed an extended lifespan and improvements across several dimensions of aging biology. By comprehensive epigenetic clock and RNA sequencing (RNA-seq) analyses, we observed a robust reduction in the epigenetic age of old mice after 3-month HPB, which was sustained even after a detachment period of 2 months. Notably, this rejuvenation effect was stronger than that observed on the more traditional, short-term HPB and is not accounted for by the effects of the surgery or changes in physical activity. We found that the transcriptomic and epigenetic profiles of long-term HPB are intermediate between young and old isochronic pairs, and that HPB positively associates with the effects of common lifespan-extending interventions and counteracts aging-related gene expression changes. Our findings suggest the presence of profound and persisting molecular rejuvenation effects after exposure to young circulation, leading to extended lifespan and healthspan.

Results

Long-term parabiosis followed by detachment extends lifespan and healthspan in mice

We used a long-term (3-month) parabiosis (either heterochronic or isochronic) period in mice, followed by detachment of the parabionts. Young mice started parabiosis at 3 months and old mice at 20 months of age (Fig. 1a). Transcriptomic and epigenetic profiling of the liver and blood was conducted to assess molecular changes resulting from HPB (Fig. 1b). For the longevity and healthspan experiments, mice were detached and allowed 1 month of recovery after parabiosis before physiological data collection (Extended Data Fig. 1a). After separation from the respective parabiosis pairs, a subset of mice were allowed to live freely until their natural death to examine the effect of parabiosis on lifespan. We observed a 6-week extension in median lifespan and a 2-week extension in maximum lifespan in old mice detached from heterochronic pairs compared to their isochronic controls (Fig. 1c). This was accompanied by an initial reduction in body weight coupled with better preservation of body weight in the final months of life (Fig. 1d). The initial drop in body weight was primarily caused by a reduction in fat mass, while preservation of body weight was due to the maintenance of both lean and fat mass later in life (Fig. 1d). These changes in body composition were independent of changes in food consumption (Extended Data Fig. 1b). In addition to improvements in body composition, old heterochronic mice showed higher voluntary cage activity than isochronic controls (Fig. 1d and Extended Data Fig. 1c).

Epigenetic age of old mice is reversed by parabiosis with a sustained effect after detachment

For epigenetic analyses, we subjected mice to the same prolonged attachment and collected tissues either immediately after the 3-month parabiosis procedure or 2 months after detachment (Extended Data Fig. 1a). We first subjected the blood and liver of the animals to reduced representation bisulfite sequencing (RRBS)[30] (Supplementary Table 1). As blood samples taken immediately after detachment contained a mixture of old and young blood (Extended Data Fig. 2a–c), we initially chose to quantify methylation changes in blood after a 2-month detachment period. At this time point, we could investigate whether epigenomic remodeling on exposure to young circulation persists without young blood contamination, as we did not observe blood crossover 2 months after detachment (Extended Data Fig. 2d). Additionally, we took liver as an example of a solid tissue to quantify the indirect effects on the methylome occurring immediately after parabiosis and after 2-month detachment.

To quantify the epigenetic age of the animals, we applied four RRBS-based epigenetic clocks to six different groups of mice: young isochronic; old isochronic; and old heterochronic mice, as well as detached variants of these three groups. Clocks used included two recently developed multi-tissue clocks[5,31], a blood-specific clock[6] and a maximum likelihood-based single-cell clock[14], which was modified to accommodate and profile epigenetic age in bulk data. Application of these clocks to blood RRBS data revealed a profound epigenetic age decrease (24 ± 3.8%) when comparing old isochronic and heterochronic pairs. Interestingly, this effect was sustained even after 2 months of detachment (reduction in age by 22.4 ± 6.4%) (Fig. 2a). Application of these same four clocks to liver data showed comparable immediate (16.8 ± 7.9%) and sustained (19.1 ± 5.4%) epigenetic age reduction as observed in blood (Fig. 2b). Together, these results indicate that long-term HPB rejuvenates the epigenome compared to isochronic pairs in both blood and liver. Moreover, these unbiased rejuvenation signals in solid organs (such as the liver) further suggest that long-term HPB acts in a systemic manner, leading to global epigenomic remodeling and organism-wide age reversal.

To confirm this epigenetic age decrease, we used a completely independent analysis platform: methylation profiling of liver samples on the recently developed mammalian methylation array[32,33] (Fig. 3 and Supplementary Table 2). We performed this profiling across three different long-term parabiosis groups (young isochronic, old isochronic and old heterochronic) along with detached pairs of each of these groups. We applied four different array-specific epigenetic clocks. Two universal clocks were used: one based on relative age standardized to maximum lifespan and one based on log-linear transformed age standardized to the age of sexual maturity. Additionally, two mouse-specific clocks were used: a broad liver-specific clock and a clock tracking the epigenetic dynamics of the developmental process in the liver. Together, all four clocks correctly predicted the age

https://doi.org/10.1038/s43587-023-00451-9

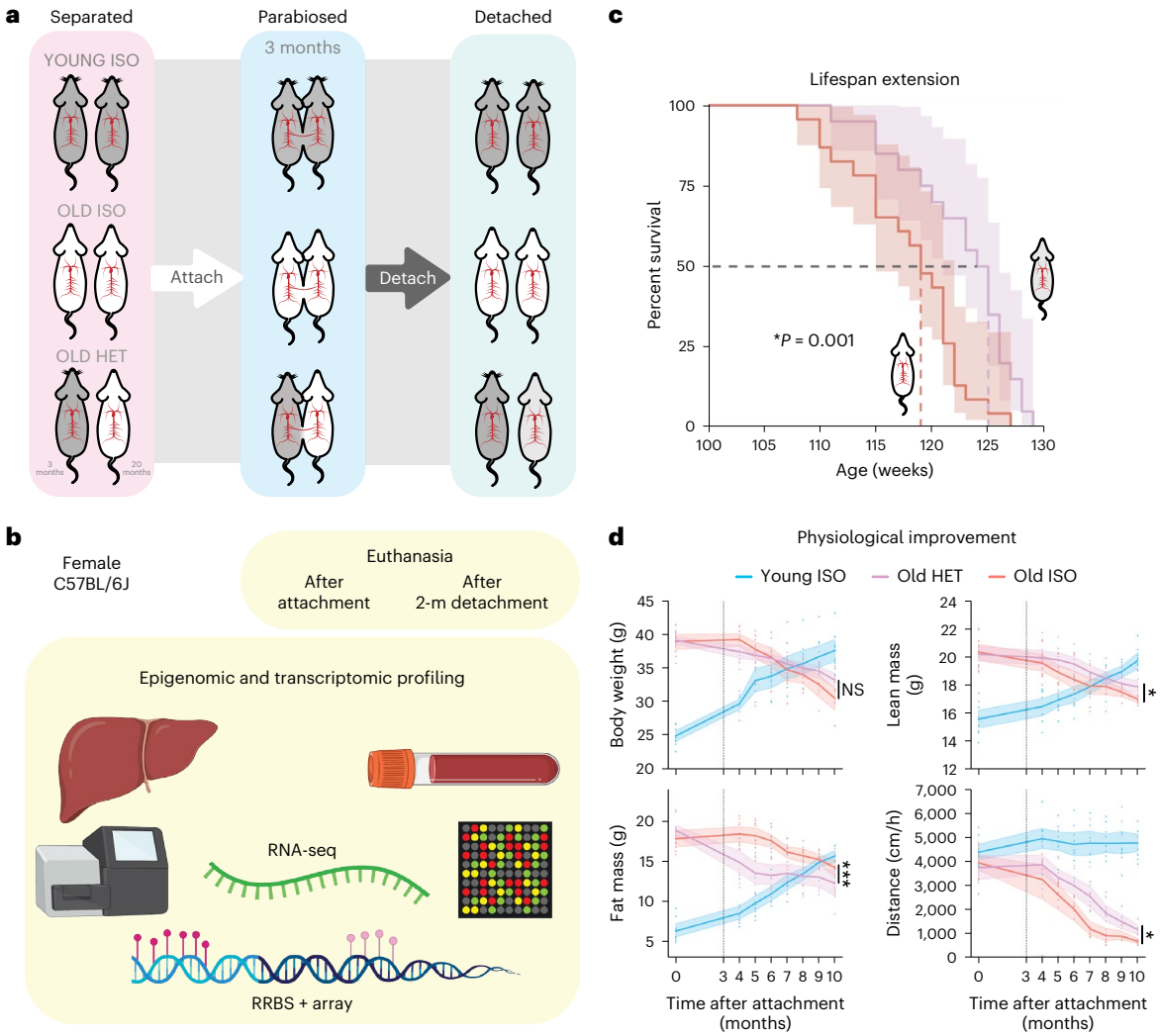

Fig. 1 | Prolonged parabiosis followed by detachment leads to extended lifespan and healthspan. a, Overview of the parabiosis and detachment model. All pairs were anastomosed for 3 months, starting at 20 months of age for old mice and 3 months of age for young mice. At 23 months, old mice were detached and the remaining lifespan was assessed. **b**, Schematic of the molecular profiling methods applied to mouse tissues. **c**, Survival curves of detached old mice from isochronic (red, $n = 23$) and heterochronic (purple, $n = 20$) pairs. Kaplan–Meier curves with 95% confidence intervals are shown. The median lifespan is highlighted with dashed lines. A log-rank test comparing the two survival curves was used for statistical analysis ($P = 0.001$). **d**, Body weight, lean mass, fat mass and cage activity measurements before parabiosis and at monthly time points starting 1 month after detachment. Mean values with 95% confidence intervals are shown. A two-tailed Welch's test was used to compare old isochronic and heterochronic groups: $P_{\text{body weight}} = 0.29$; $P_{\text{lean mass}} = 0.049$; $P_{\text{fat mass}} = 0.00092$; and $P_{\text{cage activity}} = 0.015$. 'Young ISO' denotes young mice from isochronic pairs ($n = 10$). 'Old ISO' denotes old mice from isochronic pairs ($n = 7$). 'Old HET' denotes old mice from heterochronic pairs ($n = 8$). The dashed lines show the time of detachment. *$P < 0.05$; **$P < 0.01$; ***$P < 0.001$.

of control isochronic samples with high precision and accuracy and showed a highly significant decrease in epigenetic age when comparing old heterochronic and isochronic mice (22.3 ± 4.2% reduction in age) (Fig. 3a). Again, this effect was preserved after detachment, with a slight reduction in effect size (16.1 ± 3.4% reduction in age). Moreover, results from different platforms and organs were well correlated with each other (Extended Data Fig. 3a,b). These results from an independent platform further reinforce the notion that 3-month HPB leads to a profound, sustained and systemic epigenetic rejuvenation.

We then tested the difference between the commonly used 5-week, short-term protocol and our long-term (3-month) HPB protocol. Methylation array profiling of liver tissue was performed in three groups of animals (young isochronic, old isochronic and old heterochronic) immediately after a 5-week attachment period. Only three of the four clocks applied detected a significant reduction in epigenetic age in heterochronic mice, and the effect size was dramatically smaller than in the long-term (3-month) parabiosis experiment (6.2 ± 4.1% reduction in age with short-term HPB) (Fig. 3b). Notably, the clock trained specifically on mouse liver tissues did not detect this reduction. This suggests that while short-term parabiosis may induce some moderate epigenetic remodeling leading to mild rejuvenation readouts, a longer-term treatment clearly outperforms short-term attachment when it comes to immediate and particularly sustained rejuvenation of the liver epigenome.

To further determine whether a predicted epigenetic age reversal (that is, rejuvenation) occurs in the liver, an additional analysis of delta ages (the signed difference between epigenetic and chronological age) across all groups, including an untreated, nonsurgical control group, was performed (Extended Data Fig. 3c). This revealed that heterochronic pairs, both after 3-month attachment and after the 2-month detachment period, exhibited significantly lower epigenetic age compared to their chronological age. The same trend was observed with

https://doi.org/10.1038/s43587-023-00451-9

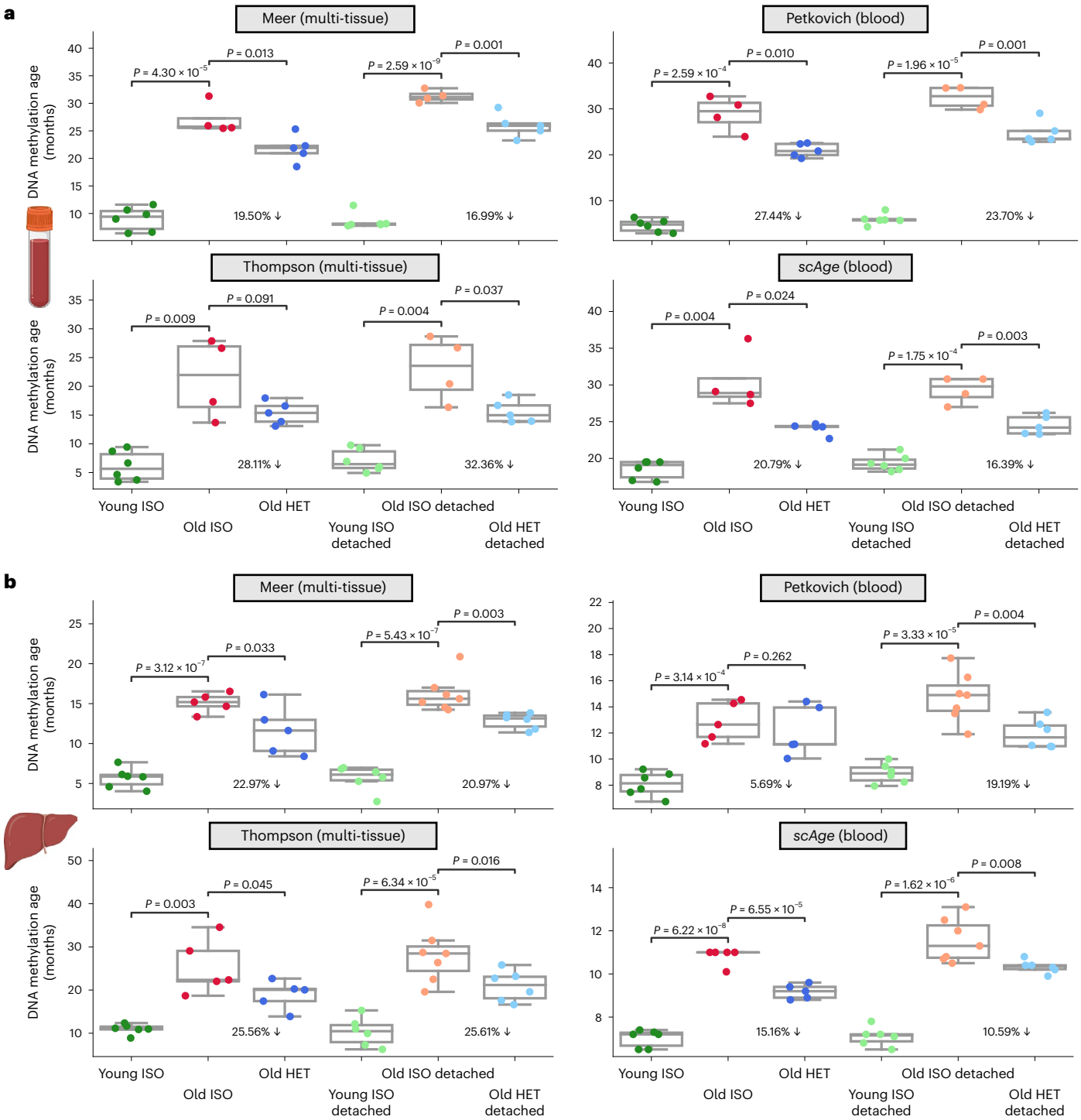

Fig. 2 | Persistent epigenetic age reversal in blood and liver on HPB assessed by RRBS-based aging clocks. a, DNA methylation age of old heterochronic blood before and after detachment plotted with isochronic young and old controls assessed by the Meer multi-tissue clock, Petkovich blood clock, Thompson multi-tissue clock and *scAge* blood clock. Young ISO $n = 6$, old ISO $n = 4$, old HET $n = 5$, young ISO detached $n = 6$, old ISO detached $n = 4$, old HET detached $n = 5$. **b**, DNA methylation age of old heterochronic liver before and after detachment plotted with isochronic young and old controls assessed with the Meer multi-tissue clock, Petkovich blood clock, Thompson multi-tissue clock and *scAge* liver clock. Young ISO $n = 6$, old ISO $n = 5$, old HET $n = 5$, young ISO detached $n = 6$, old ISO detached $n = 6$, old HET detached $n = 6$. 'Young ISO' denotes young mice from isochronic pairs. 'Old ISO' denotes old mice from isochronic pairs. 'Old HET' denotes old mice from heterochronic pairs. 'Detached' denotes detached old mice from isochronic or heterochronic pairs. The box plots represent the median, 25–75 percentiles and 1.5× the interquartile range (IQR). One-tailed Welch's *t*-tests assuming unequal variances were used for the statistical analyses.

attached mice from the short-term parabiosis experiments, but the effect size was dramatically stronger on long-term treatment. In addition, the lack of difference between the old isochronic group and the old untreated control (Extended Data Fig. 3c) gives confidence that the parabiosis surgery itself does not alter the epigenome. We also tested this in young mice comparing the young isochronic group to a young nonsurgical control group (Extended Data Fig. 3d). Again, we found no significant difference with the age-matched nonsurgical control mice.

https://doi.org/10.1038/s43587-023-00451-9

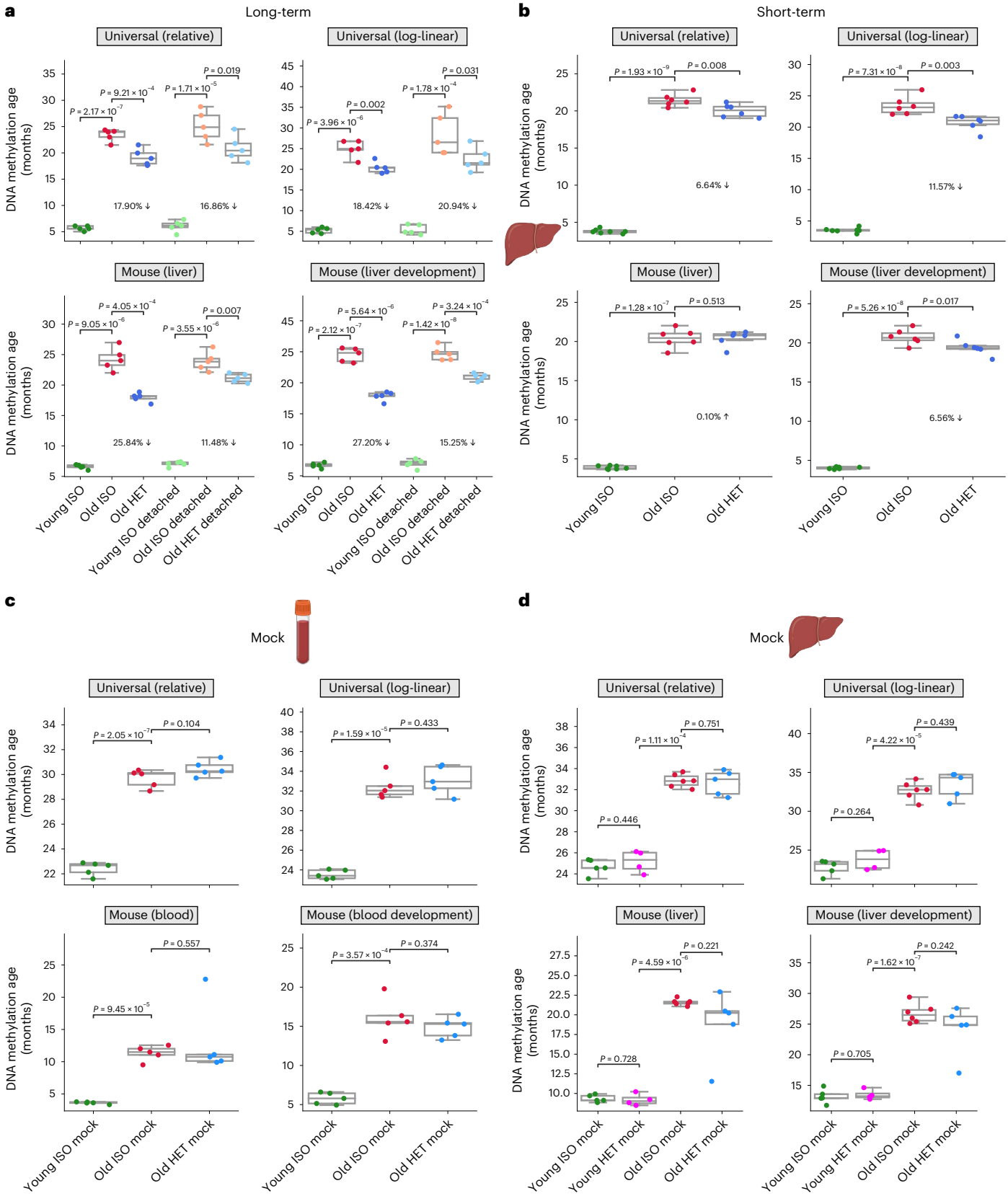

Fig. 3 | Sustained epigenetic age reversal in liver on HPB assessed by microarray-based aging clocks. a, Epigenetic age of long-term (3-month) parabiosis liver samples from old heterochronic attached or detached mice, plotted with young and old isochronic controls, based on the universal relative age mammalian, universal log-linear-transformed age mammalian, liver and liver development clocks. $n = 5$ per group. **b**, Epigenetic age of short-term (5-week) parabiosis liver samples from old heterochronic attached mice, plotted with young and old isochronic controls, based on the same clocks as in **a**. $n = 6$ per group. **c**,**d**, Epigenetic age of short-term (5-week) mock parabiosis blood (**c**) and liver (**d**) samples from old heterochronic attached mice, plotted with young and old isochronic controls, based on the same clocks as in **a**. $n = 5$ per group for heterochronic mice and $n = 6$ per group for isochronic mice. The box plots represent the 25–75 percentiles and 1.5× IQR. One-tailed Welch's *t*-tests were used for the statistical analysis.

Additionally, we found that mean methylation was consistent among samples, suggesting that targeted epigenetic remodeling, manifesting itself in decreased epigenetic clock age, occurs as a result of long-term HPB (Extended Data Fig. 4).

A generally accepted mechanism for the health effects of HPB is youthful blood sharing. However, physical activity, especially in older populations, can affect epigenetic age[34]. The influence of physical activity on the epigenetic effects of HPB has been discussed but, to our knowledge, not measured. In this study, we developed a 'mock' parabiosis model to attach mice without blood sharing for 5 weeks, matching our short-term HPB (Extended Data Fig. 5a–c). We observed a 32% decrease in voluntary cage activity in the old isochronic pairs compared to the young isochronic pairs (Extended Data Fig. 5c,d). In contrast, activity in the heterochronic pair was similar to the young isochronic groups. Moreover, the heterochronic group had a trend of increased vertical activity when compared to the old isochronic group. Despite the changes in physical activity, mock parabiosis did not alter epigenetic age in either blood or livers (Fig. 3c,d), suggesting that blood sharing is the prerequisite to obtain changes in the epigenetic age in the HPB model.

In addition to using clocks on the epigenetic data, we explored the impact of HPB on the promoter methylation levels of individual genes. We identified several genes with significant differential mean promoter methylation across old isochronic and heterochronic mice, in both attached and detached samples (Extended Data Fig. 6d). Among the genes, we observed decreased promoter methylation in *Ubl5*, which has previously been linked to lifespan modulation in nematodes[35], as well as *Mpped1*, which was previously identified as an age-regulated gene in the brain across humans, macaques and mice[36].

Taken together, we report that a systemic rejuvenation occurs in old animals on exposure to youthful circulation, as assessed by eight distinct epigenetic clocks across two independent DNA methylation analysis platforms. Furthermore, we showed that the slowing of epigenetic age is sustained even after a 2-month detachment period. These results present the first example of a systemic in vivo rejuvenation quantified by molecular biomarkers in mice.

Gene expression analyses reveal pathways responsive to long-term parabiosis

Given the notable epigenetic age reversal, we sought to concurrently elucidate the transcriptomic changes that occur as a result of HPB. We performed RNA-seq analyses of liver tissues in old isochronic and heterochronic mice, as well as in detached groups of both conditions, followed by differential gene expression and gene set enrichment analyses (GSEA) (Fig. 4a). Using the Hallmark, Kyoto Encyclopedia of Genes and Genomes (KEGG), REACTOME and Gene Ontology (GO) Biological Process (BP) gene sets obtained from the Molecular Signatures Database (MSigDB)[37,38], we computed normalized enrichment scores (NES) comparing isochronic and heterochronic samples immediately after the 3-month parabiosis period, as well as after 2 months of detachment (Fig. 4a). Among samples taken immediately after the attachment period, we observed strong enrichment of the oxidative phosphorylation and mitochondrial biogenesis gene sets in heterochronic mice. Interestingly, oxidative phosphorylation is known to be disrupted during the aging process[39]. Within this context, our results indicate that HPB may reverse some of the age-associated decline commonly associated with this critical energy production pathway. We also observed depletion of inflammatory and interferon-γ (IFNγ) response gene sets in heterochronic mice (that is, enrichment of inflammation in old isochronic mice). IFNγ protein level is known to increase with age in some tissues (particularly in T cells)[40], and inflammation is one of the crucial hallmarks of aging[2] associated with the development of various age-related pathologies, including cancer[41], Alzheimer's disease[42] and chronic kidney disease[43]. These results further support the rejuvenating effect of HPB on murine transcriptomic profiles.

To investigate whether transcriptomic changes at the gene set level are sustained, we compared the GSEA results from samples taken immediately after the attachment period to those after 2 months of detachment (Fig. 4a). We observed a strong positive correlation between the enrichment scores obtained for the attached and detached groups (Spearman $\rho = 0.72$, $P < 10^{-16}$); the top significantly enriched pathways in the detached analyses were common in identity and direction with those in the attached group, suggesting that transcriptomic changes in the liver resulting directly from HPB are largely sustained even after prolonged detachment (Fig. 4a). Of note, the NES and number of significantly enriched gene sets were generally decreased in the detached group, despite the same number of samples being analyzed (Fig. 4a). This may indicate the gradual reduction of the HPB effect after detachment.

We also conducted global differential gene expression analyses, comparing isochronic and heterochronic samples after the 3-month attachment period or after the 2-month detachment. We identified 1,044 significantly ($P_{adj} < 0.05$) upregulated and 1,855 downregulated genes in the post-attachment comparison (Fig. 4b), compared to 876 upregulated and 1,034 downregulated genes in the detached comparison (Fig. 4c). Together, these data suggest that the liver transcriptome is rejuvenated on HPB and that this rejuvenation largely persists even after a 2-month detachment.

Dimensionality reduction reveals intermediate molecular phenotypes resulting from HPB

Given the high dimensionality of epigenomic and transcriptomic data, we opted to use principal component analysis (PCA) to embed and visualize samples in two-dimensional space. We observed that HPB samples clustered between young and old isochronic samples, closer to the young samples than the old (Fig. 5a). While clustering of short-term parabiosis also showed an intermediate transcriptomic profile for old heterochronic mice, these samples clustered much closer to the old isochronic group (Fig. 5b). Together with the epigenetic clock data, this further suggests that long-term parabiosis is a much more potent age reversal intervention compared to short-term parabiosis.

We also performed PCA on the RRBS methylation data from liver and blood samples (Fig. 5c–h and Extended Data Fig. 6a–c). We analyzed methylation at individual CpG sites, as well as through concatenation into two types of genomic regions known to be functionally influenced by cytosine methylation: promoters (Supplementary Table 3) and gene bodies (Supplementary Table 4). Across both tissues, we observed that old heterochronic samples clustered in between old and young isochronic samples when analyzing over 1 million highly covered CpGs (Fig. 5c,d). These results are especially pronounced when collapsing methylation to promoters and gene bodies, where heterochronic samples fall perfectly between the two isochronic groups (Fig. 5e–h).

Altogether, application of dimensionality reduction to our data suggests that old heterochronic mice have transcriptomic and epigenetic profiles intermediate between young isochronic and old isochronic mice. This effect is apparent across both liver and blood. Moreover, we observed that long-term parabiosis produces a more profound shift in transcriptomic profiles toward a young state compared to short-term parabiosis. This further indicates that global and sustained transcriptomic and epigenomic remodeling occurs as a result of long-term but not short-term HPB.

Gene expression changes induced by HPB mirror longevity intervention signatures and oppose aging

To further assess if HPB results in systemic rejuvenation of the transcriptome, we compared the identified gene expression changes with signatures associated with lifespan extension and aging, obtained through a previously published meta-analysis of multiple publicly available datasets. They include liver-specific gene signatures of individual

https://doi.org/10.1038/s43587-023-00451-9

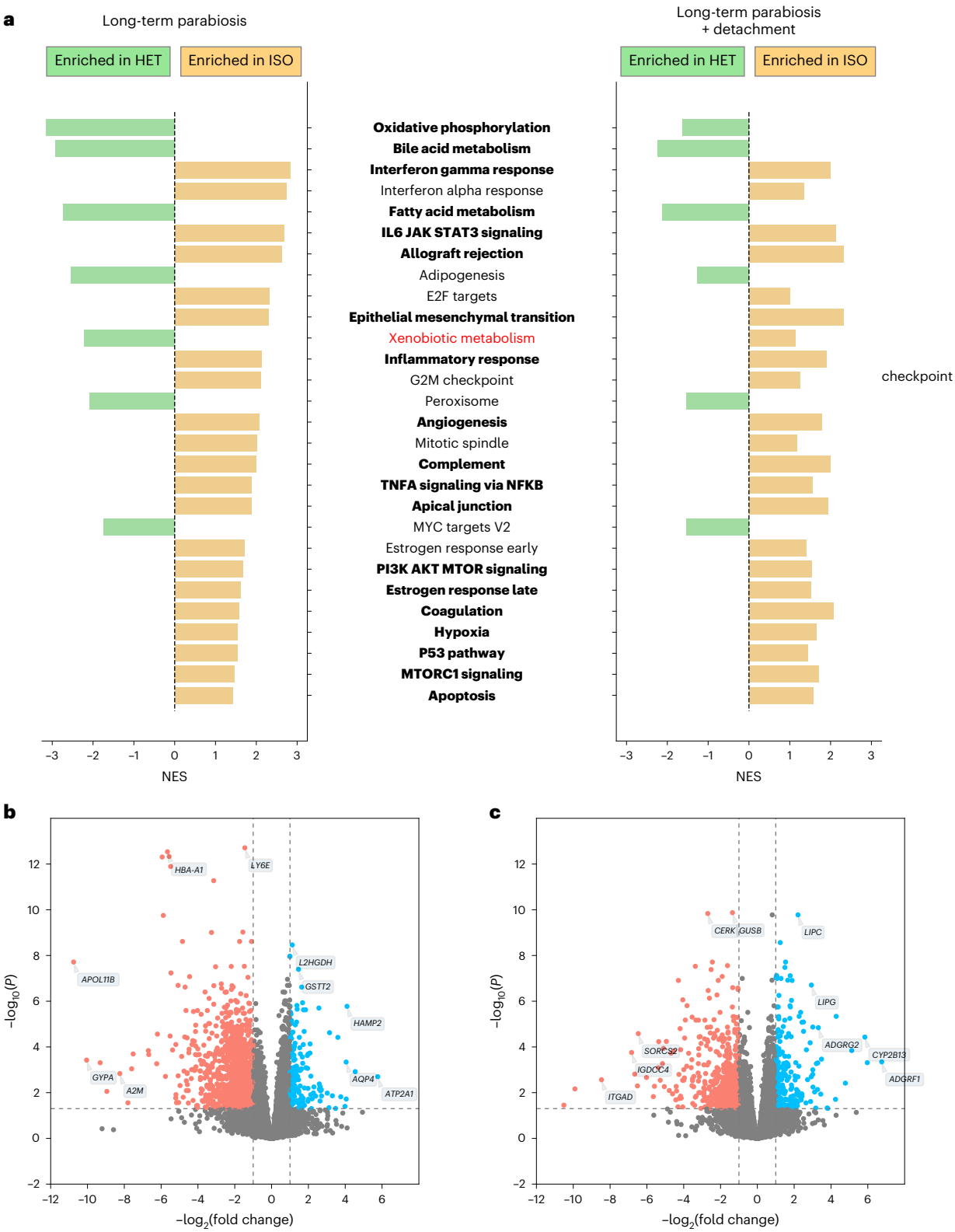

Fig. 4 | Transcriptomic analyses of HPB reveal unique pathway enrichment and differential expression patterns. a, GSEA of old isochronic versus old heterochronic mice (left), as well as of detached old isochronic versus detached old heterochronic mice (right). Hallmark gene sets ($n = 50$) were used as input to the GSEA. Only significant enrichments in the attached groups ($P_{adj} < 0.05$) are shown. The gene sets shown in green signify pathways enriched in the heterochronic samples, and orange those enriched in the isochronic samples. The terms in bold signify pathways that are significantly enriched in the same direction in both attached and detached groups. The terms in normal black font signify pathways that are enriched in the same direction in both attached and detached groups but only significantly so in the attached comparison. The term in red signifies a pathway that is enriched in different directions in the attached and detached comparisons. Significant gene sets are ranked from top to bottom based on the absolute value of the NES in the attached group. **b**,**c**, Volcano plot of differentially expressed genes in attached (**b**) and detached (**c**) old heterochronic ($n = 3$) and old isochronic ($n = 3$) mice. Several highly significant genes are shown in each plot. Genes shown in red are significantly downregulated in heterochronic mice, while genes shown in blue are significantly upregulated in heterochronic mice, after correction for multiple testing. A two-tailed Benjamini–Hochberg-corrected false discovery rate was calculated to compare groups.

https://doi.org/10.1038/s43587-023-00451-9

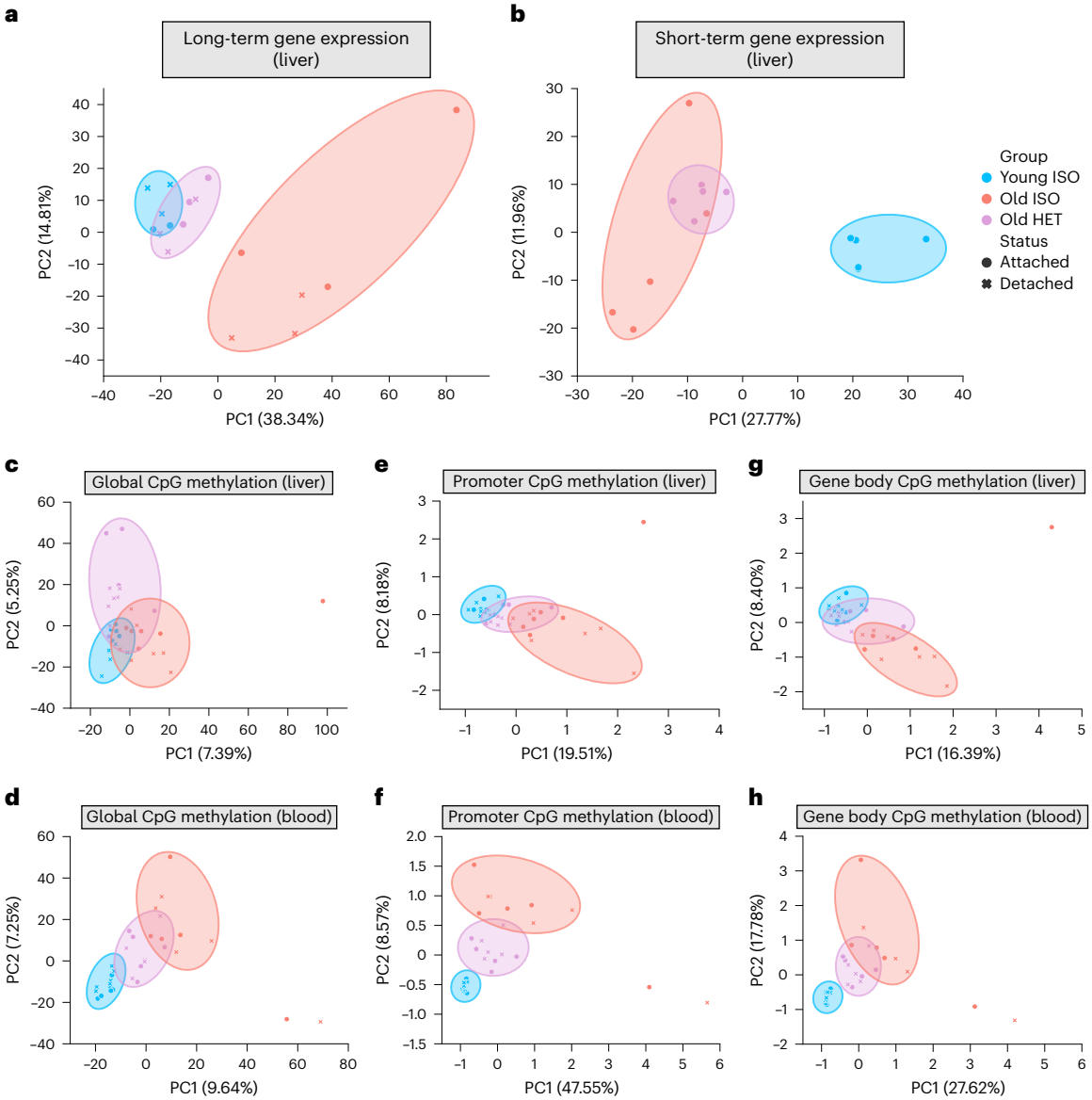

Fig. 5 | Dimensionality reduction highlights rejuvenated molecular profiles after HPB. a, PCA of liver RNA-seq data of mice after long-term parabiosis or 2 months after detachment ($n = 3$ per group). **b**, PCA of liver RNA-seq data of mice after short-term parabiosis ($n = 3$ per group). **c**, PCA of liver RRBS data across all highly covered common CpGs (1,014,243 CpGs, $n = 5$–7 per group). **d**, PCA of blood RRBS data across all highly covered common CpGs (1,014,243 CpGs, $n = 5$ or 6 per group). **e**, PCA of liver RRBS data across gene promoters (11,842 promoters, $n = 5$–7 per group). **f**, PCA of blood RRBS data across gene promoters (11,842 promoters, $n = 5$ or 6 per group). **g**, PCA of liver RRBS data across gene bodies (13,811 gene bodies, $n = 5$–7 per group). **h**, PCA of blood RRBS data across gene bodies (13,811 gene bodies, $n = 5$ or 6 group). 'Young ISO' denotes young isochronic mice. 'Old ISO' denotes old isochronic mice. 'Old HET' denotes old heterochronic mice. Attached refers to samples taken immediately after the parabiosis period, while detached refers to samples taken after 2 months of detachment. The percentages of variance explained by the first two principal components are shown in parentheses on the axes.

interventions (such as CR and mutations leading to growth hormone (GH) deficiency), gene expression changes shared across different lifespan-extending interventions and genes whose expression is associated with the quantitative effect of interventions on maximum and median lifespan. In contrast, aging signatures reflect age-related transcriptomic changes observed in the liver of mice and rats, as well as multi-tissue age-related alterations in each of these species.

We evaluated the association between parabiosis-induced changes and these signatures using a previously described GSEA-based approach[44,45]. In heterochronic samples taken immediately after the 3-month parabiosis or after the 2-month detachment period, we observed a strong and significant negative association with three aging signatures, including the mouse liver, rat multi-tissue and mouse multi-tissue aging signatures (adjusted permutation $P < 5 \times 10^{-4}$) (Fig. 6a). On the contrary, there was a strong positive association between HPB in old mice and four out of five signatures from lifespan-extending interventions, including positive enrichment for median and maximum lifespan signatures and those for CR and GH deficiency (adjusted permutation $P < 5 \times 10^{-4}$). Of note, significant absolute NES were consistently decreased in magnitude (20.4 ± 11.3% reduction) in detached samples compared to samples taken immediately after the long-term parabiosis period (Fig. 6a). Consistent with the functional enrichment analysis presented earlier, this suggests that most transcriptomic changes are sustained after the detachment period, but the magnitude of the rejuvenating effect may be gradually diminished over time.

https://doi.org/10.1038/s43587-023-00451-9

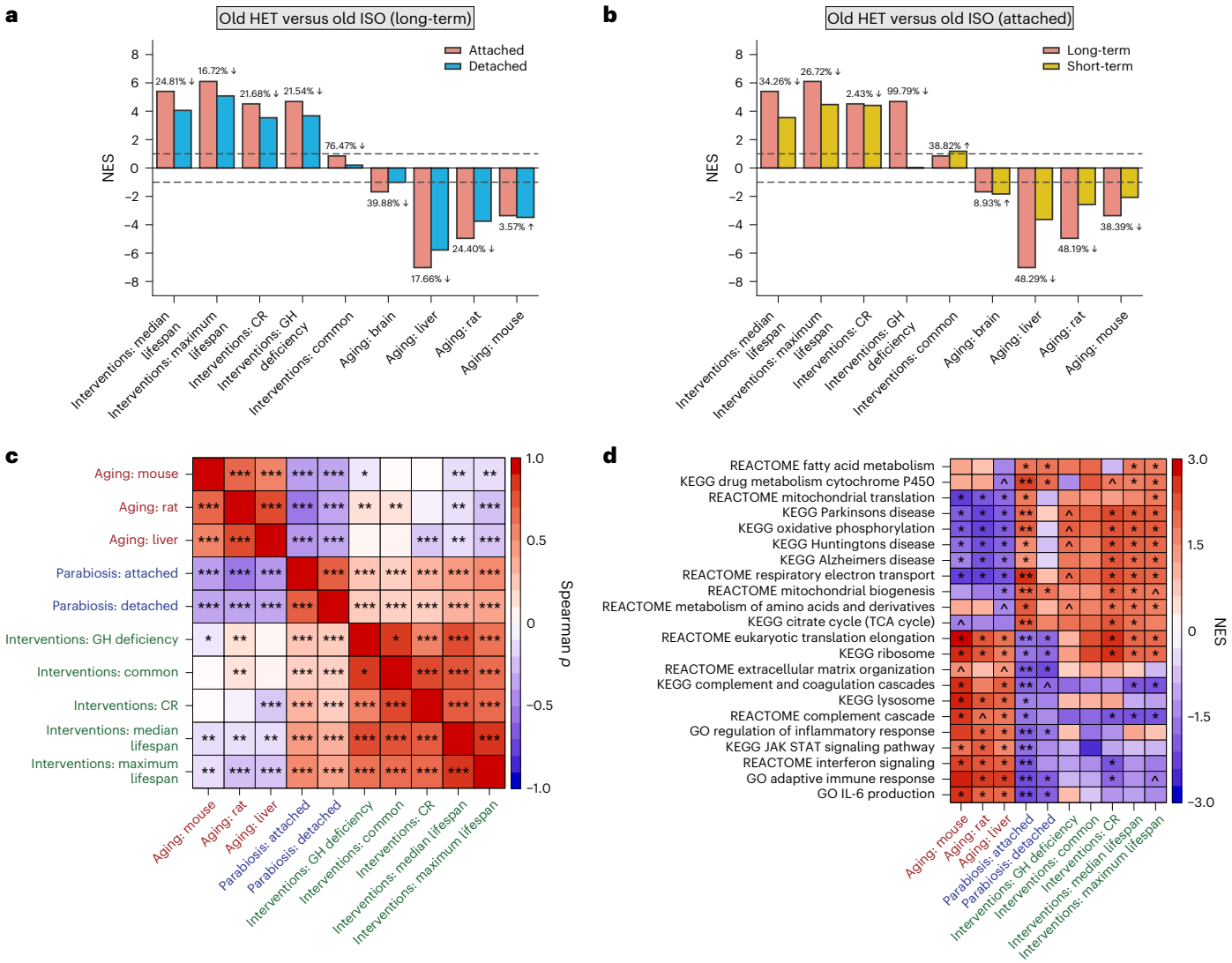

Fig. 6 | The transcriptomic signatures of HPB align with longevity interventions and oppose aging. a, Association between gene expression changes induced by long-term parabiosis with (blue) and without (red) a 2-month detachment period, and signatures of aging- and lifespan extension. The latter include gene signatures of individual interventions (CR and GH deficiency), common intervention signatures (interventions: common) and signatures associated with an effect on lifespan (maximum and median lifespan). The percentage decrease comparing the attached and detached samples is shown for each pair of bars. **b**, Association between gene expression changes induced by long-term (red) and short-term (yellow) parabiosis without detachment and signatures of aging and lifespan extension. The signatures analyzed are the same as in **a**. **c**, Spearman correlation matrix of gene expression signatures associated with aging (red labels), lifespan extension (green labels) and HPB (blue labels). **d**, Functional enrichment analyses of gene expression signatures. Only functions significantly associated with at least one signature are shown. Cells are colored based on NES. The entire list of enriched functions is provided in Supplementary Table 5. *P* values were generated using GSEA. $^{\wedge}P_{adj} < 0.1$; $^{*}P_{adj} < 0.05$; $^{**}P_{adj} < 0.01$; $^{***}P_{adj} < 0.001$.

To refine the molecular resolution of longevity effects based on the duration of the parabiosis intervention, we also performed transcriptomic signature analysis for short-term (5-week) parabiosis samples. In accordance with the previous observations, we observed significant positive associations of HPB with several signatures of lifespan extension, while aging signatures demonstrated the opposite effect (Fig. 6b). This suggests that short-term parabiosis leads to important transcriptomic changes similar to those produced by established longevity interventions. However, the magnitude of association for short-term parabiosis was greatly reduced compared to long-term attachment. Therefore, long-term parabiosis seems to induce more profound lifespan-extending and rejuvenating effects at the level of gene expression and DNA methylation, highlighting the enhanced effect of the long-term HPB protocol.

To investigate mutual associations between the changes induced by HPB, lifespan extension and aging, we calculated the Spearman correlation coefficients of the log fold change of genes for each pair of signatures. Consistent with the GSEA-based association analysis, the effects induced by HPB in old mice clustered together with the changes induced by lifespan-extending interventions and were positively correlated with them (Spearman $\rho = 0.22$; $P_{adj} < 2 \times 10^{-5}$) but negatively correlated with aging-related changes (Spearman $\rho = -0.3$; $P_{adj} < 3 \times 10^{-9}$) (Fig. 6c). Interestingly, based on our data, the negative association between aging and parabiosis in older animals was even more substantial than between aging and existing lifespan-extending interventions, such as CR (Spearman $\rho = -0.22$).

To understand which gene sets are responsible for the age reversal and lifespan-extending effects of HPB, we performed functional GSEA

for the above-mentioned aging and longevity signatures (Fig. 6d and Supplementary Table 5). We observed that some functions that were upregulated in response to parabiosis, including the tricarboxylic acid cycle, respiratory electron transport chain and mitochondrial biogenesis, were also upregulated by lifespan-extending interventions, but downregulated during aging. At the same time, functions related to the immune response, such as interferon signaling and complement and coagulation cascades, were significantly downregulated both in response to HPB and established lifespan-extending interventions, but upregulated with age. Therefore, HPB in old mice seems to counteract aging by activating genes related to metabolism and cellular respiration while inhibiting the inflammatory response, like other longevity interventions.

In addition, to understand how the effects of parabiosis compare across the transcriptome and epigenome, we analyzed the correlation of the changes in promoter methylation and RNA expression comparing old isochronic and heterochronic mice, in both the attached and detached experimental groups (Extended Data Fig. 7a). Interestingly, we found that while the same readout modalities correlated well with each other across the attached and detached groups (RRBS $r = 0.67$; RNA $r = 0.72$), there was a much smaller correlation between parabiosis-induced changes when comparing the transcriptome and epigenome directly ($r = 0.2$). We also looked at the directional concordance of differentially expressed and methylated genes across readout types and attached and detached groups (Extended Data Fig. 7b). Again, we found very strong concordance when comparing the same assay types (RRBS or RNA) across attached and detached experiments (RRBS concordance = 88%, RNA concordance = 92%), but significantly less concordance when comparing RRBS with RNA in the same experiment (attached concordance = 65%, detached concordance = 60%, with 50% concordance signifying random effects). Taken together, we found that the effect of HPB is largely conserved between attached and detached groups when accounting for each modality separately. However, there was a smaller concordance between the magnitude and direction of changes induced by HPB when comparing promoter methylation and expression levels of individual genes. This suggests that parabiosis is not acting entirely through the epigenome to affect gene transcription; instead, several layers of biological regulation are involved in the global rejuvenation effect we observe.

To summarize, we observed that HPB indeed rejuvenated old animals systemically and this was supported by both epigenetic and transcriptomic remodeling induced by this intervention. Excitingly, signature analyses of HPB profiles recapitulate the gene expression effects of established lifespan-extending interventions, pointing to the potential utility of derivatives of this therapy in promoting healthy longevity.

Individual gene expression dynamics reveal putative longevity-associated mechanisms for HPB

To uncover the potential mechanisms underlying the rejuvenation effects we observed on long-term parabiosis, we investigated the individual genes regulated in response to HPB and their association with longevity and aging based on the gene expression signatures (Fig. 7). We found that 27–45% of genes significantly changed in response to long-term and short-term HPB were also significantly associated with maximum and median lifespan extension in the same direction (Fisher's exact test $P < 0.03$ for all models of HPB). Additionally, there was a significant overlap of genes downregulated in response to long-term HPB and upregulated with age according to all tested aging signatures (Fisher's exact test $P < 0.004$ for long-term attached and detached groups).

Among genes upregulated by long-term HPB in both attached and detached models, we identified *Sirt3* (attached $P_{adj} < 0.047$) (Fig. 7a). *Sirt3* deficiency is known to promote cancer[46] and aging[47,48], while its overexpression has resulted in the decrease of reactive oxygen species levels and improvement of regenerative capacity in aged stem cells[48]. Not surprisingly, its expression in liver is upregulated by many longevity interventions, including CR and GH deficiency ($P_{adj} < 0.049$), and is positively associated with the effect of interventions on median and maximum lifespan extension in mice ($P_{adj} < 10^{-14}$) (Fig. 7a).

Other important hits, connecting the effects of HPB with the mechanisms of established longevity interventions, are genes involved in glutathione metabolism, such as *Gstt2*, encoding for glutathione S-transferase theta 2. *Gstt2* was upregulated in response to long-term HPB and remained increased after detachment (detached $P_{adj} < 0.008$) (Fig. 7b). These findings point to some putative specific longevity mechanisms induced by long-term HPB. Methionine metabolism had an important role in the regulation of longevity; an increased blood level of glutathione is an important biomarker of caloric[49] and methionine restriction[50]. Consistent with this data, the expression of *Gstt2* demonstrated significant positive association with the effect of various lifespan-extending interventions ($P_{adj} < 4 \times 10^{-12}$ for the signatures of median and maximum lifespan extension) (Fig. 7b).

Among genes downregulated by HPB and longevity interventions but upregulated with age, we identified several involved in the immune response such as *C1qb*, which encodes for one of the complement subcomponents (Fig. 7c). *C1qb* was downregulated in response to long-term HPB both immediately after attachment and after 2 months of detachment ($P_{adj} < 0.03$) (Fig. 7c). This gene is positively associated with aging in the liver and brain in both mice and rats ($P_{adj} < 0.05$ for all aging signatures). At the same time, its expression in murine liver is downregulated by CR ($P_{adj} = 0.028$) and demonstrates negative association with median and maximum lifespan extension induced by interventions ($P_{adj} < 0.023$) (Fig. 7c). We confirmed the gene expression dynamics observed via RNA-seq for *Sirt3*, *Gsst2* and *C1qb* by quantitative PCR with reverse transcription (RT–qPCR), and observed concordant changes in protein expression as detected by western blotting (Fig. 7 and Extended Data Fig. 6e,f).

We also observed a significant increase in *Tert* expression after long-term HPB ($P_{adj} = 4.3 \times 10^{-5}$), which appeared to be sustained in detached samples ($P_{adj} = 0.0014$) (Extended Data Fig. 8a). Although *Tert*, encoding for telomerase reverse transcriptase, does not demonstrate significant upregulation in response to various longevity interventions, the overexpression of this gene by itself has resulted in lifespan extension in healthy mice without induction of cancer[51].

Another interesting hit was *Dnmt3b*, which encodes one of the key enzymes involved in de novo methylation of the genome. We observed a significant decrease in *Dnmt3b* expression when comparing isochronic and heterochronic mice from long-term and short-term parabiosis (Extended Data Fig. 8a). This effect was also sustained in detached samples from long-term HPB. While de novo methylation occurs primarily during embryogenesis and is responsible for a rejuvenation event around the time of gastrulation, this finding may additionally implicate *Dnmt3b* as a key driver in the modulation of epigenetic remodeling induced by HPB[13,14,52]. We also observed significant downregulation of other genes induced by both short-term and long-term HPB, including *Ly6e*, *Lmna* and *Pld1* (Extended Data Fig. 8a). Notably, the expression of these genes was at the same time negatively associated with the effect of longevity interventions on median and maximum lifespan, indicating that they may also mediate the beneficial effect of HPB. Consistent with our other data, the gene effect size was strongest in long-term attached samples, intermediate in long-term detached and lowest in short-term attached samples, again reinforcing the utility of a long-term attachment period for transcriptomic rejuvenation.

To determine whether the observed gene expression changes were related to upstream epigenetic changes, we examined the mean promoter methylation levels of these genes (Extended Data Fig. 8b). Interestingly, we observed minimal differences in promoter methylation across samples for these genes, despite observing significant changes at the transcriptional level. This suggests that, at least for some

https://doi.org/10.1038/s43587-023-00451-9

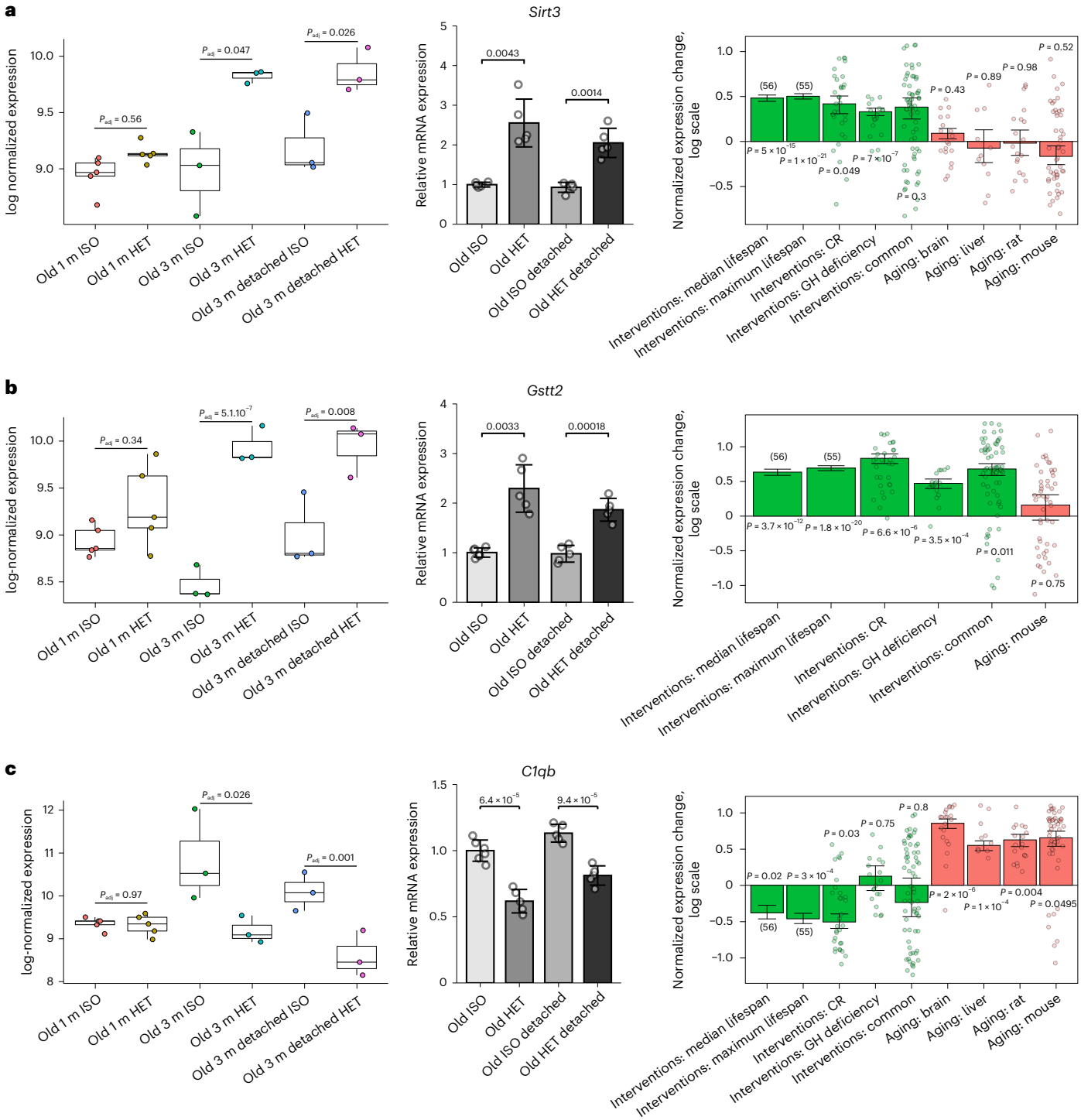

Fig. 7 | Gene expression analyses hint at putative rejuvenation mechanisms of long-term HPB. a–**c**, Expression of *Sirt3* (**a**), *Gstt2* (**b**) and *C1qb* (**c**) in mice subjected to parabiosis by RNA-seq analyses (left), RT–qPCR analyses (middle) and in response to established lifespan-extending interventions and aging (right). Left: for each gene, normalized expression in logarithmic scale is shown across different parabiosis groups: short-term isochronic (old 1 m ISO, $n = 5$) and heterochronic (old 1 m HET, $n = 5$) mice, long-term attached isochronic (old 3 m ISO, $n = 3$) and heterochronic mice (old 3 m HET, $n = 3$), long-term detached isochronic (old 3 m detached ISO, $n = 3$) and heterochronic mice (old 3 m detached HET, $n = 3$). Adjusted *P* values, indicating the difference in expression for each pair of isochronic and heterochronic mice, were calculated using a preplanned two-tailed Student's *t*-test. The box plots represent the median, 25–75 percentiles and 1.5× IQR. Middle: for the RT–qPCR of each gene, each group has $n = 5$ biological replicates. The *P* value between connecting bars was calculated with a two-tailed Student's *t*-test. Right: for every signature associated with lifespan-extending interventions (green) and aging (red), the means of the normalized log fold changes or slopes (for the signatures of the median and maximum lifespan) are presented. The error bars denote ± 1 s.e. Adjusted *P* values, indicating the difference of expression change from zero, were calculated with a mixed-effect linear model.

genes, changes in promoter methylation are largely not responsible for changes in gene expression patterns in our data. Furthermore, for the genes that were found to have significant differential promoter methylation across isochronic and heterochronic mice in attached and detached samples (Extended Data Fig. 6d), none had significant changes in expression levels across any comparison. This finding further supports the notion that parabiosis acts through multiple layers of regulation, instead of only through methylome modifications.

Lastly, we also observed strong negative enrichment of senescence-associated secretory phenotype (SASP) genes (Supplementary Table 6) in heterochronic mice immediately after long-term parabiosis ($P_{adj} = 4 \times 10^{-4}$) (Extended Data Fig. 9a). Expression of SASP-related genes is known to increase with age[53], suggesting that HPB ameliorates the pro-inflammatory phenotype of the aging liver. This negative enrichment was also observed in detached heterochronic samples ($P_{adj} = 0.01$) and in short-term heterochronic samples ($P_{adj} = 0.008$), but the effect in both was noticeably smaller (Extended Data Fig. 9b,c). Gene-specific analyses among several key SASP genes (*Cdkn1a*, *Il1r1*, *Cxcl13*, *Igfbp7*, *Tgfb1*) further revealed significant expression changes between old heterochronic and isochronic mice after 3-month attachment and after 2-month detachment, but not after short-term attachment (Extended Data Fig. 9d).

Together, these results suggest that long-term HPB causes profound transcriptomic change at the level of gene sets and individual genes associated with longevity and rejuvenation. STRING clustering of upregulated and downregulated genes further indicates commonalities in the regulatory gene ensembles that are modified as a result of HPB (Extended Data Fig. 10a,b). The observed shared genes and pathways point to the existence of crucial and interconnected molecular mechanisms driving the rejuvenation effect of long-term HPB, some of which have been described in this work.

Discussion

The history of HPB dates back to the mid-twentieth century and it has re-emerged as an important model in aging research since 2005[19,26,54]. In the past, most of these studies have focused primarily on phenotypes, such as tissue regeneration, brain function and stem cell characteristics. It has remained enigmatic whether this intervention could systematically reverse the epigenetic age of organisms and, moreover, whether the effects of HPB last after a prolonged detachment period. One challenge in this regard has been that the duration of circulatory system attachment in animals was too short to observe robust differences in epigenetic age. By adapting a long-term parabiosis protocol to include detachment, and by using precise molecular biomarkers of aging, we have demonstrated for the first time that exposure to the young circulatory system leads to persistent and systemic slowing of epigenetic aging. Notably, this effect correlates with a longer lifespan, improved physiological parameters and a globally rejuvenated epigenome and transcriptome.

We found that multiple epigenetic clocks point to slowing of epigenetic age, and the effect was observed independently using two different profiling platforms: high-throughput sequencing (that is, RRBS) and microarrays. Importantly, we found that HPB decreases the epigenetic age acceleration (that is, delta age) even compared to non-parabiosed control animals, suggesting that this effect is an actual reversal of epigenetic age rather than an amelioration of surgery-induced age acceleration. It is important to note that while almost all clocks showed significant epigenetic age reversal, some clocks showed only marginal differences. This most often happens when there is incongruence between the tissues used for clock training and the actual tissues tested, that is, the blood clock is not as precise in assessing epigenetic age in the liver.

The degree of rejuvenation we observed in our work is consistent with previous studies, which showed that HPB ameliorates aging phenotypes of tissues other than the blood, such as the muscle, liver and nervous system. While our study was under review, Yankova et al. published data using a similar HPB approach followed by detachment, where they showed a striking decrease in the lifespan of the young parabiont[55]. Although our lifespan analyses focused only on the old detached mice, our data and those of Yankova et al. were confirmatory. We both show a similar, modest increase in lifespan in old mice following detachment from HPB, despite differences in mouse strain, sex and exact timing of surgical interventions.

It is probable that cells and molecules in circulation contribute to the effect of parabiosis on solid organs and therefore affect cells resident to these tissues[22,56–58]. Our finding further fortifies the view that aging is a systemic process[59]. Additionally, we observed that gene expression changes induced by HPB in old mice (compared to isochronic controls) were negatively correlated with changes induced by aging, but positively correlated with changes induced by longevity interventions. Consistent with a recent study examining the effect of short-term parabiosis on single-cell gene expression[60], our findings indicate that what we observed is in fact multi-omic, systemic and sustained biological rejuvenation. Although our methylation clock analyses showed a decrease in epigenetic age up to 30% from HPB, the lifespan extension effect on the detached mice, while still significant, was not as strong. This discrepancy may be the result of the many comorbidities occurring later in the mouse lifespan.

The complexity of the HPB model lends several caveats beyond sharing of 'youthful' factors to understanding its biology. This includes, but is not limited to, contributions from cellular chimerism, surgical stress or changes in physical activity. Regarding cellular chimerism, we did not believe this to be a factor in the maintenance of the healthspan and reduced epigenetic age in our model. Although previous studies on congenic mouse strains reported that 3–5% of the blood from the parabiont remains in the body after 7 weeks of detachment[27], our model showed limited evidence of young cells in the old bone marrow or in circulation after the detachment period. The lack of bone marrow chimerism with HPB is in agreement with previous reports[29]. Therefore, we believe that extensions of healthspan and epigenetic alterations are based on the anti-aging effects during anastomosis, with minimal contribution from the lingering young blood cells after detachment. Another effect of HPB, often discussed but seldom tested, is the effect on physical activity. We developed a nonsurgical mock parabiosis model, enabling us to physically attach mice without blood sharing. We were surprised to see greater cage activity in the mock heterochronic pairs compared to the mock old isochronic group, which warranted further analysis to determine its effect on epigenetic remodeling. Despite the increased physical activity, we did not see any changes in epigenetic age, ruling out activity as a confounding variable to influence epigenetic age predictions in our HPB model. Lastly, we showed no effect of the parabiosis surgery itself on epigenetic age. While there are subtle differences in surgical methods across the parabiosis literature, it is important to know that our model was not altering epigenetic age when compared to age-matched, non-surgery controls. Together, these data help support the theory of blood factor transfer being the primary mechanism of rejuvenation.

There have been attempts to identify the components involved and some factors from young blood like oxytocin were reported to recapitulate the physiological rejuvenation effect[61,62]. After bone marrow transplantation, the blood of recipients maintains the epigenetic age of the donors, indicating that there may be factors intrinsic to blood cells and their precursors contributing to this effect[63]. Another possibility could be that aged organisms accumulate damage, which can be effectively diluted by young blood during parabiosis experiments. This hypothesis is supported by a recent experiment that involved replacing the blood plasma with saline containing 5% albumin, leading to enhanced muscle repair and hippocampal neuroregeneration[64]; however, this has yet to be demonstrated using a longitudinal model.

It is critical to note that there has been no evidence yet from aging clocks favoring either of these two hypotheses.

Overall, our findings reveal a robust decrease in epigenetic age on long-term HPB, which remains strongly significant after a period of prolonged detachment. This is coupled with a strong positive correlation between parabiosis and longevity interventions and a negative correlation between parabiosis and aging based on several gene expression signatures. Gene set and pathway analyses revealed a positive enrichment of the tricarboxylic acid cycle, oxidative phosphorylation, mitochondrial biogenesis and fatty acid metabolism pathways, as well as depletion (that is, negative enrichment) of IFNγ and inflammatory response pathways in old heterochronic mice. Additionally, several longevity-mediated genes were identified, including *Gstt2*, *Sirt3*, *C1qb* and *Tert*, which showed sustained expression changes after long-term parabiosis. Importantly, we validated that long-term (3-month) parabiosis is much more effective at rejuvenating the transcriptome and epigenome of mice compared to short-term (5-week) parabiosis. This long-lasting rejuvenation effect of HBP in old mice leads to the extension of healthspan and lifespan even after this traumatic surgery, and produces molecular profiles intermediate between young and old mice. Although we observed a strong conservation of effects using both modalities (RRBS and RNA-seq) across attached and detached groups, the concordance between the two omic readouts was smaller, probably indicating that parabiosis simultaneously affects different layers of biological regulation. At present, several interventions or biological events have been shown to reverse epigenetic age, including rejuvenation during early embryogenesis, rejuvenation by pharmaceutical treatment and rejuvenation via reprogramming factor expression. Given this, it would be interesting to investigate molecular commonalities resulting from these interventions, helping to design perturbations that recapitulate the rejuvenation effect without requiring a complex and impractical surgery such as parabiosis.

To conclude, our results indicate that epigenetic age can be systemically decelerated in a sustained manner after long-term exposure to young circulation. This opens exciting new avenues for research on parabiosis and its more translational derivatives for organismal rejuvenation.

Methods

Mouse models

All animal care followed the guidelines and was approved by the Institutional Animal Care and Use Committees at Duke Medical Center. Female C57BL/6J (wild-type) mice were used at 3 months and 20 months of age. The selection of female mice was based on better temperament when conjoined and better survival rates in females compared to males after the surgeries. All mice were acquired from the National Institute on Aging colony. Details about mouse number and survival across the cohorts and surgery protocols are shown in the table found in Extended Data Fig. 1a.

Parabiosis and detachment surgery

Parabiosis was performed as described previously[65], with modifications to the length of the protocol. Parabiosis surgery was carried out using 3- or 20-month-old female mice. Under isoflurane anesthesia, incisions were made through the skin and fascia on opposing lateral sides of the abdomen of each mouse followed by suturing of the fascia and suturing of the skin. Suturing the underlying fascia allows anastomosis and angiogenesis through the natural wound healing process[65]. Mouse pairs were prescreened to minimize differences in body size but were otherwise chosen randomly. All pairs were maintained together for 3 months, then euthanized or detached for further analysis. The detachment surgery was performed under isoflurane anesthesia, separating the pairs by reversing the attachment site. Once both mice were separated, the skin and fascia were sutured closed. For the longevity analysis, all detached mice were allowed 1 month of recovery before entry into the study in an attempt to account for any premature deaths due to surgical complications. Experimental groups for the longevity study were isochronic old (old ISO) and heterochronic old (old HET). Mice used for longevity studies were not used for the healthspan studies to prevent confounding effects, and were allowed to live until natural death or recommendation of euthanasia by a veterinarian. For the healthspan studies, all mice were detached after the 3-month parabiosis period and phenotypic and functional data collection started 1 month after detachment to allow for surgical recovery. Experimental groups included isochronic young (young ISO), isochronic old (old ISO) and heterochronic old (old HET). The same groups were used for the detachment cohorts. For the epigenetic analyses, all mice were anastomosed for 3 months then analyzed while still attached or analyzed 2 months after detachment. Experimental groups included isochronic young (young ISO), isochronic old (old ISO) and heterochronic old (old HET). The same groups were used for the detachment cohorts and annotated with 'detached' in our datasets and figures. We previously showed a shared blood supply at 5 weeks[23] and in this study showed some continued sharing at 3 months after surgery using flow cytometry, as shown in Extended Data Fig. 2. To isolate the effects of blood sharing and physical attachment, we performed mock parabiosis (Extended Data Fig. 5). For mock parabiosis, we similarly selected mice as for regular parabiosis. Both mice were anesthetized using isoflurane and opposing lateral sides of the abdomen were sutured from elbow to knee (the same distance as standard parabiosis) to create a physical attachment between the two mice. Importantly, for the mock parabiosis, no incisions were made to the skin or fascia before attachment thus preventing the generation of shared vasculature. We confirmed separation of circulation by testing the blood glucose response in both parabionts to an intraperitoneal glucose bolus delivered to one of the partners. All mock parabiosis pairs were attached for 5 weeks. Further details about the mock parabiosis experiments are shown in Extended Data Fig. 5.

Genomic DNA and total RNA isolation

Five to seven samples were taken per group for RRBS, five to six DNA samples for the microarray analyses and three to five samples for the RNA-seq analyses. The detailed number in each experimental group can be found in Supplementary Table 1. DNA from samples was isolated using the DNeasy Blood & Tissue Kit (catalog no. 69506, QIAGEN) and then eluted from columns in 100 µl of 10 mM Tris-HCl buffer, pH 8.0. Then, 2 µl of RNase A (Thermo Fisher Scientific) was added to each sample. Samples were incubated at room temperature for 2 min and isolated genomic DNA was purified using the Genomic DNA Clean & Concentrator-10 kit (catalog no. D4011, Zymo Research). DNA was eluted in 25 µl of 10 mM Tris-HCl buffer, pH 8.0, and quantified using a Qubit 2.0 (catalog no. AM2271, Thermo Fisher Scientific). RNA from liver samples was eluted using the Invitrogen Ambion RNAqueous Total RNA Isolation Kit (catalog no. AM1912, Invitrogen) in 60 µl of nuclease-free water and quantified using the Qubit 2.0.

RRBS library preparation and data processing

RRBS libraries were prepared according to the protocol established previously[6], using 100 ng of DNA for each sample. Each library included ten samples. To avoid an overlap of batch effect and age-related changes, we randomized samples into nine separate libraries (Supplementary Table 1). Liver and blood samples were analyzed separately. The libraries were sequenced using an Illumina HiSeq 2500, with 150-bp paired-end reads. Twenty percent of the mouse genomic DNA library was spiked in to compensate for low complexity of the libraries. RNA samples were sequenced separately. Adapter removal and quality trimming for the analysis of the DNA methylation reads were performed using TrimGalore v.0.4.1 according to previously established protocols[5,6,66]. For the genomic DNA methylation analyses, the trimmed reads were mapped to the mouse genome (GRCm38.p2/mm10) using Bismark v.0.15.0 (ref. 66).

Coverage files outputted by Bismark were then used for further analyses. To ensure high accuracy and precision in methylation levels, CpG sites that had less than 10-read coverage were filtered out. When combining liver and blood samples into one matrix, a total of 1,014,243 CpGs were covered at a depth greater than 10 across all samples.

For the promoter methylation analyses, the promoter region of each gene was determined as (−1500, +500) bp from the transcription start site following the direction of transcription by using the RefSeq annotation file MmRefSeqTSS.sga (https://ccg.epfl.ch/mga/mm10/refseq/refseq.html). Mean promoter methylation levels were calculated for each gene by taking the average of all CpGs covered in a particular promoter. To reduce noise from promoters with minimal CpG coverage, only promoters that had at least five CpG sites with valid data were retained for downstream analysis. This resulted in coverage of 11,842 promoters across all liver and blood RRBS samples. Gene body methylation analyses were conducted by concatenating all CpGs within a particular gene body (from transcription start site to transcription end site) and averaging methylation, just as in the promoter methylation analyses (again with a ≥5 CpG filter). This resulted in coverage of 13,811 gene bodies across all blood and liver samples.

Application of mouse epigenetic clocks to the RRBS datasets

Four clocks were applied to the RRBS dataset to characterize epigenetic age, including two whole-lifespan multi-tissue clocks (Meer clock trained on 416 samples across 40 age groups, ranging from 1 week to 35 months and Thompson clock trained on 1,189 samples ranging from approximately 1 week to 35 months)[5,31], a blood-based clock (trained on 141 mice across 16 age groups, ranging from 3 to 35 months)[6] and a recently developed maximum likelihood-based single-cell clock[14], modified to accommodate bulk data (Fig. 2). Epigenetic clock analyses for conventional ElasticNet-based clocks[5,6,31] were performed exactly according to the protocols outlined in the respective original research articles.

In the case of the single-cell clock (*scAge)*, several modifications were applied compared to its original application[13]. Indeed, in the original *scAge* application to sparse single-cell data, single-cell profiles were predominantly binary, but this is not the case with bulk RRBS data. Bulk methylation levels are often fractional, given that many reads coming from different cells usually cover a single CpG. Therefore, to account for this biologically meaningful fractional methylation distribution, no forced binarization of RRBS profiles was performed before running the algorithm. This enabled epigenetic age predictions without modification to the input data. Given the targeted nature of RRBS, the top 25% age-associated CpGs per sample were used for predictions. As training data to the modified *scAge* framework, we used bulk C57BL/6J RRBS data from Thompson et al.[31]. Two CpG-specific reference tables were created: (1) bulk blood RRBS methylation profiles from 50 normally fed C57BL/6J mice across 1,202,751 CpG sites; and (2) bulk liver RRBS methylation profiles from 29 normally fed C57BL/6J mice across 1,042,996 CpG sites on the positive strand. Based on dimensionality reduction analyses, two blood samples and one liver sample that were evident outliers were removed from the downstream epigenetic aging analyses (Fig. 5 and Supplementary Table 1). A Welch's one-tailed *t*-test assuming unequal variances was used for statistical testing.

Application of mouse epigenetic clocks to the DNA microarray dataset

We analyzed five samples in each group with the recently developed Infinium array HorvathMammalMethylChip40 and its expanded version HorvathMammalMethylChip320 (refs. 32,33). Six clocks were applied in our analysis, including two clocks based on mouse liver (mouse liver and mouse liver development), two clocks based on mouse blood (mouse blood and mouse blood development), a universal mammalian clock based on age relative to maximum lifespan (universal relative) and a universal mammalian clock based on log-linear-transformed age (universal log-linear) (Fig. 3). The mouse (liver development) clock was similar to the mouse (liver) clock, except that sites were subselected based on changes occurring during development in this organ. The epigenetic age data are in Supplementary Table 2. Welch's one-tailed *t*-tests assuming unequal variances were used for statistical testing.

RNA-seq analysis of HPB

Paired-end RNA-seq for mouse liver samples was performed on an Illumina NovaSeq 6000 S4 platform with 100-bp read length. Reads were mapped with STAR (v.2.5.2b)[67] and counted via featureCounts (v.1.5)[68]. Data were passed through RLD transformation[69] and genes with |transformed normalized count |< 1 were filtered out. This left 22,772 genes, which were used for dimensionality reduction and further analyses (Figs. 4–7). For the signature association analysis and the identification of longevity-associated genes perturbed by HPB, we further filtered out genes with low numbers of reads, keeping only the genes with at least ten reads in at least 50% of the samples, which resulted in 12,374 detected genes according to Entrez annotations.

Differential gene expression analyses

Differential expression analyses (DEA) were conducted using DEseq2 on normalized count data. All samples were concatenated to a single data frame and normalized jointly before analysis to minimize the batch effect bias. A total of 15,481 valid genes were obtained when conducting DEA on long-term parabiosis samples comparing old isochronic and old heterochronic mice. Similarly, 14,522 valid genes were obtained when conducting DEA on long-term detached parabiosis samples comparing old detached isochronic and old detached heterochronic mice. These data were used to generate the volcano plots for the attached and detached samples in Fig. 4. Volcano plots were generated using the package bioinfokit v.2.0.6.

For the signature association analyses (Fig. 6) and investigation of longevity-associated genes regulated by HPB (Fig. 7), differential expression of genes in response to HPB compared to isochronic parabiosis was further analyzed using edgeR[70] separately for the long-term attached, long-term detached and short-term attached models. Obtained *P* values were adjusted for multiple comparison with the Benjamini–Hochberg method[71]. The relative log expression method was used to obtain normalized expression of genes[72].

Dimensionality reduction

To identify the trajectories of molecular profiles resulting from HPB, we conducted dimensionality reduction via PCA on gene expression (RNA-seq) and methylation (RRBS) data (Fig. 5). For the gene expression analyses, we used normalized, RLD-transformed gene count values from the liver across 22,272 genes in both short-term and long-term parabiosis samples (Fig. 5a,b). For sequencing-based methylation data, we used information at 1,014,243 highly covered (≥10×) CpG sites in liver and blood samples. These data were then collapsed into 11,842 promoters and 13,811 gene bodies, each covered by at least 5 CpGs to ensure reliable mean methylation measurements. The percentage of the variance explained by the first two principal components was extracted and is shown across panels in Fig. 5.

Association of signature-based gene expression changes induced by parabiosis, aging and lifespan-extending interventions

The gene expression signatures of lifespan-extending interventions, including the signatures of CR, the signatures of GH deficiency, common gene expression changes across different interventions and the signatures associated with the effect of interventions on median and maximum lifespan, were obtained from Tyshkovskiy et al.[44]. Aging signatures, including the liver signature and the mouse and rat multi-tissue signatures, were obtained via a meta-analysis of age-related gene expression changes[45]. Association of gene expression log fold changes

associated with parabiosis, lifespan extension and aging were assessed using correlation and GSEA[37]. For the correlation analysis, a Spearman correlation metric was calculated using the top 200 statistically significant genes for each pair of signatures. Clustering was subsequently performed with a complete hierarchical approach.

For the GSEA-based association analysis, we used an algorithm developed by Tyshkovskiy et al.[44]. First, for every signature we specified 250 genes with the lowest *P* values and separated them into upregulated and downregulated genes. These lists were subsequently considered as gene sets. Then, we ranked genes differentially expressed in response to parabiosis based on their *P* values, calculated as described in the following section. Afterwards, we calculated NES separately for upregulated and downregulated lists of gene sets as described by Tyshkovskiy et al.[44] and defined the final NES as a mean of the two. To calculate the statistical significance of the obtained NES, we performed permutation testing where we randomly assigned genes to the lists of gene sets, maintaining their size. To get the *P* value of the association between parabiosis and a certain signature, we used 5,000 permutations and calculated the frequency of random final NES that are larger in magnitude than the observed final NES. To adjust for multiple testing, we performed a Benjamini–Hochberg correction[67]. Final NES for the association of HPB response with various longevity and aging signatures were used to generate the barplots (Fig. 6a,b). Overlap between significant differentially expressed genes in response to HPB and lifespan-extending interventions or aging was assessed using a Fisher's exact test separately for sets of upregulated and downregulated genes.

Functional enrichment analysis

For the identification of enriched functions distinguishing isochronic and heterochronic mice, we performed functional GSEA[37] on a pre-ranked list of genes based on $\log_{10}(P)$ corrected by the sign of regulation, calculated as:

$$-\log(P) \times \mathrm{sgn}(\log \text{ fold change})$$

where the *P* value and log fold change of a certain gene were obtained from the edgeR output; sgn is the signum function (equal to 1, −1 and 0 if the value is positive, negative or equal to 0, respectively). REACTOME, KEGG and GO BP ontologies from the MSigDB were used as the gene sets for GSEA. The GSEA algorithm was performed separately for long-term attached and detached models via the fgsea package in R with 5,000 permutations. A *q* value cutoff of 0.1 was used to select statistically significant functions.

A similar analysis was performed for gene expression signatures associated with aging and lifespan extension. A heatmap colored according to NES was built for manually chosen, statistically significant functions (Fig. 6c,d). Clustering of functions was performed with a complete hierarchical approach and Spearman correlation distance.

For the parabiosis samples, we also conducted additional GSEA using the Hallmark gene sets downloaded from the MSigDB. We used a recent Python GSEA implementation, gseapy v.1.0.0, to perform gene set enrichment. Only Hallmark gene sets with Benjamini–Hochberg-adjusted *P* values below 0.05 in the attached comparison are shown in Fig. 4a. GSEA was conducted separately for long-term attached and long-term detached samples, with 5,000 gene set permutations for statistical testing. Hallmark terms significantly enriched in the same direction across both attached and detached comparisons are shown in bold. Terms enriched in the same direction, but only significantly so in the attached comparison, are shown in normal black font. The term enriched in opposite directions across attached and detached comparisons is shown in red.

Cage activity

Voluntary activity was tested in the open field arena (Omnitech) illuminated at 340 lux as previously described by Huffman et al.[73]. Mice were placed individually into the open field and baseline locomotion was monitored over 60 min.

Protein, western blotting and RT–qPCR mRNA expression

RNA isolation, complementary DNA synthesis and mRNA expression were performed as described previously[65]. All primers used in this manuscript are: *Sirt3*-Forward: GAGCGGCCTCTACAGCAAC *Sirt3*-Reverse: GGAAGTAGTGAGTGACATTGGG; *Gstt2*-Forward: TTCCTGTACTCAAAGACGGAAGC *Gstt2*-Reverse: CTGCCACCTGGTACTTGGAAC; *C1qb*-Forward: CGTCGGCCCTAAGGGTACT *C1qb*-Reverse: GGGGCTGTTGATGGTCCTC. Protein isolation and western blotting were performed as described previously[74]. Primary antibodies used were as follows: Sirt3 (catalog no. 5490, Cell Signaling Technology); C1qb (catalog no. NBP2-92455, Novus Biologicals); Gstt2 (catalog no. H00002953-D01P, Thermo Fisher Scientific); and pan-tubulin (catalog no. 2194, Cell Signaling Technology). The secondary antibody was an anti-rabbit IgG, horseradish peroxidase-linked antibody (catalog no. 7074, Cell Signaling Technology).

Statistics and reproducibility

No statistical method was used to predetermine sample size. Two blood samples and one liver sample that were evident outliers in the PCA were removed from downstream epigenetic aging analyses. The excluded samples are also >3 standard deviations away from the mean. Experimental mice were randomized after initial screening to minimize extreme body weight differences between pairings. Investigators were blinded to group allocations during the experiments and outcome assessments after detachment.

Computational analyses were performed in Python v.3.9.15, running with numpy v.1.23.5 and pandas v.1.5.2. Statistical analyses for epigenetic ages were performed with a one-tailed Welch's *t*-test, implemented in scipy v.1.9.3. Statistical analyses for gene expression were performed with custom models from DEseq2 v.3.13 and edgeR v.3.34.1 in R v.4.0.3 (ref. 70). Statistical analyses of gene expression signatures, GSEA and epigenetic age profiling were performed as documented above.

For the statistical evaluation of body composition, activity and food consumption data (Fig. 1d and Extended Data Fig. 1b,c), we used a custom test based on random simulations. We generated a randomly simulated point for each time point of old isochronic samples using the average and s.d. of the old isochronic samples of each time point. In a similar way, we generated another randomly simulated point for each time point of the old heterochronic samples. This process resulted in a simulated time series for old heterochronic samples and for old isochronic samples. We assessed these time series by summarizing the differences for simulated old isochronic–old heterochronic pairs for all time points. Repeating the whole procedure 100,000 times, we calculated the *P* value as the proportion of the cases when the difference between both time series was greater than 0, if the null hypothesis was 'old isochronic > old heterochronic', and less than 0, if the null hypothesis was 'old isochronic < old heterochronic'. If the *P* value was less than 0.05, we rejected the null hypothesis and considered the difference significant. The null hypothesis was 'old isochronic > old heterochronic' in the case of body weight, lean mass, distance and vertical activity, and 'old isochronic < old heterochronic' in the case of fat mass and food consumption. Data distributions were assumed to be normal but this was not formally tested.

Reporting summary

Further information on research design is available in the Nature Portfolio Reporting Summary linked to this article.

Data availability

The sequencing data obtained in this study are deposited with the Gene Expression Omnibus under accession no. GSE224447. The data

used to generate the graphs can be found in the accompanying source data files. Source data for Figs. 1–7 and Extended Data Figs. 1–10 are provided with the paper.

References

1. Brett, J. O. & Rando, T. A. Alive and well? Exploring disease by studying lifespan. *Curr. Opin. Genet. Dev.* **26**, 33–40 (2014).
2. López-Otín, C., Blasco, M. A., Partridge, L., Serrano, M. & Kroemer, G. The hallmarks of aging. *Cell* **153**, 1194–1217 (2013).
3. López-Otín C., Blasco, M. A., Partridge, L., Serrano, M. & Kroemer, G. Hallmarks of aging: an expanding universe. *Cell* **186**, 243–278 (2023).
4. Horvath, S. DNA methylation age of human tissues and cell types. *Genome Biol.* **14**, R115 (2013).
5. Meer, M. V., Podolskiy, D. I., Tyshkovskiy, A. & Gladyshev, V. N. A whole lifespan mouse multi-tissue DNA methylation clock. *eLife* **7**, e40675 (2018).
6. Petkovich, D. A. et al. Using DNA methylation profiling to evaluate biological age and longevity interventions. *Cell Metab.* **25**, 954–960 (2017).
7. Olova, N., Simpson, D. J., Marioni, R. E. & Chandra, T. Partial reprogramming induces a steady decline in epigenetic age before loss of somatic identity. *Aging Cell* **18**, e12877 (2019).
8. Fahy, G. M. et al. Reversal of epigenetic aging and immunosenescent trends in humans. *Aging Cell* **18**, e13028 (2019).
9. Horvath, S. et al. Reversing age: dual species measurement of epigenetic age with a single clock. Preprint at *bioRxiv* https://doi.org/10.1101/2020.05.07.082917 (2020).
10. Lu, Y. et al. Reprogramming to recover youthful epigenetic information and restore vision. *Nature* **588**, 124–129 (2020).
11. Rando, T. A. & Chang, H. Y. Aging, rejuvenation, and epigenetic reprogramming: resetting the aging clock. *Cell* **148**, 46–57 (2012).
12. Sarkar, T. J. et al. Transient non-integrative expression of nuclear reprogramming factors promotes multifaceted amelioration of aging in human cells. *Nat. Commun.* **11**, 1545 (2020).
13. Kerepesi, C., Zhang, B., Lee, S.-G., Trapp, A. & Gladyshev, V. N. Epigenetic clocks reveal a rejuvenation event during embryogenesis followed by aging. *Sci. Adv.* **7**, eabg6082 (2021).
14. Trapp, A., Kerepesi, C. & Gladyshev, V. N. Profiling epigenetic age in single cells. *Nat. Aging* **1**, 1189–1201 (2021).
15. Lunsford, W. R., McCay, C. C., Lupien, P. J., Pope, F. E. & Sperling, G. Parabiosis as a method for studying factors which affect aging in rats. *Gerontologia* **7**, 1–8 (1963).
16. McCay, C. M., Pope, F. & Lunsford, W. Experimental prolongation of the life span. *Bull. N. Y. Acad. Med.* **32**, 91–101 (1956).
17. Pope, F., Lunsford, W. & McCay, C. M. Experimental prolongation of the life span. *J. Chronic Dis.* **4**, 153–158 (1956).
18. Baht, G. S. et al. Exposure to a youthful circulation rejuvenates bone repair through modulation of β-catenin. *Nat. Commun.* **6**, 7131 (2015).
19. Conboy, I. M. et al. Rejuvenation of aged progenitor cells by exposure to a young systemic environment. *Nature* **433**, 760–764 (2005).
20. Loffredo, F. S. et al. Growth differentiation factor 11 is a circulating factor that reverses age-related cardiac hypertrophy. *Cell* **153**, 828–839 (2013).
21. Ruckh, J. M. et al. Rejuvenation of regeneration in the aging central nervous system. *Cell Stem Cell* **10**, 96–103 (2012).
22. Villeda, S. A. et al. Young blood reverses age-related impairments in cognitive function and synaptic plasticity in mice. *Nat. Med.* **20**, 659–663 (2014).
23. Vi, L. et al. Macrophage cells secrete factors including LRP1 that orchestrate the rejuvenation of bone repair in mice. *Nat. Commun.* **9**, 5191 (2018).
24. Rebo, J. et al. A single heterochronic blood exchange reveals rapid inhibition of multiple tissues by old blood. *Nat. Commun.* **7**, 13363 (2016).
25. Middeldorp, J. et al. Preclinical assessment of young blood plasma for Alzheimer disease. *JAMA Neurol.* **73**, 1325–1333 (2016).
26. Conboy, M. J., Conboy, I. M. & Rando, T. A. Heterochronic parabiosis: historical perspective and methodological considerations for studies of aging and longevity. *Aging Cell* **12**, 525–530 (2013).
27. Wright, D. E., Wagers, A. J., Gulati, A. P., Johnson, F. L. & Weissman, I. L. Physiological migration of hematopoietic stem and progenitor cells. *Science* **294**, 1933–1936 (2001).
28. Donskoy, E. & Goldschneider, I. Thymocytopoiesis is maintained by blood-borne precursors throughout postnatal life. A study in parabiotic mice. *J. Immunol.* **148**, 1604–1612 (1992).
29. Ho, T. T. et al. Aged hematopoietic stem cells are refractory to bloodborne systemic rejuvenation interventions. *J. Exp. Med.* **218**, e20210223 (2021).
30. Meissner, A. et al. Reduced representation bisulfite sequencing for comparative high-resolution DNA methylation analysis. *Nucleic Acids Res.* **33**, 5868–5877 (2005).
31. Thompson, M. J. et al. A multi-tissue full lifespan epigenetic clock for mice. *Aging* **10**, 2832–2854 (2018).
32. Lu, A. T. et al. Universal DNA methylation age across mammalian tissues. *Nat. Aging* https://doi.org/10.1038/s43587-023-00462-6 (2023).
33. Arneson, A. et al. A mammalian methylation array for profiling methylation levels at conserved sequences. *Nat. Commun.* **13**, 783 (2022).
34. Fiorito, G. et al. DNA methylation-based biomarkers of aging were slowed down in a two-year diet and physical activity intervention trial: the DAMA study. *Aging Cell* **20**, e13439 (2021).
35. Durieux, J., Wolff, S. & Dillin, A. The cell-non-autonomous nature of electron transport chain-mediated longevity. *Cell* **144**, 79–91 (2011).
36. Loerch, P. M. et al. Evolution of the aging brain transcriptome and synaptic regulation. *PLoS ONE* **3**, e3329 (2008).
37. Subramanian, A. et al. Gene set enrichment analysis: a knowledge-based approach for interpreting genome-wide expression profiles. *Proc. Natl Acad. Sci. USA* **102**, 15545–15550 (2005).
38. Liberzon, A. et al. The molecular signatures database (MSigDB) hallmark gene set collection. *Cell Syst.* **1**, 417–425 (2015).
39. Lesnefsky, E. J. & Hoppel, C. L. Oxidative phosphorylation and aging. *Ageing Res. Rev.* **5**, 402–433 (2006).
40. Bandres, E. et al. The increase of IFN-gamma production through aging correlates with the expanded $CD8^{+high}CD28^{-}CD57^{+}$ subpopulation. *Clin. Immunol.* **96**, 230–235 (2000).
41. Leonardi, G. C., Accardi, G., Monastero, R., Nicoletti, F. & Libra, M. Ageing: from inflammation to cancer. *Immun. Ageing* **15**, 1 (2018).
42. Lai, K. S. P. et al. Peripheral inflammatory markers in Alzheimer's disease: a systematic review and meta-analysis of 175 studies. *J. Neurol. Neurosurg. Psychiatry* **88**, 876–882 (2017).
43. Amdur, R. L. et al. Inflammation and progression of CKD: the CRIC study. *Clin. J. Am. Soc. Nephrol.* **11**, 1546–1556 (2016).
44. Tyshkovskiy, A. et al. Identification and application of gene expression signatures associated with lifespan extension. *Cell Metab.* **30**, 573–593 (2019).
45. Tyshkovskiy, A. et al. Distinct longevity mechanisms across and within species and their association with aging. *Cell* https://doi.org/10.1016/j.cell.2023.05.002 (2023).
46. Gonzalez Herrera, K. N., Finley, L. W. & Haigis, M. C. The role of SIRT3 in regulating cancer cell metabolism. *BMC Proc.* **6**, P18 (2012).
47. Benigni, A. et al. *Sirt3* deficiency shortens life span and impairs cardiac mitochondrial function rescued by *Opa1* gene transfer. *Antioxid. Redox Signal.* **31**, 1255–1271 (2019).
48. Brown, K. et al. SIRT3 reverses aging-associated degeneration. *Cell Rep.* **3**, 319–327 (2013).

49. Lang, C. A., Wu, W. K., Chen, T. & Mills, B. J. Blood glutathione: a biochemical index of life span enhancement in the diet restricted Lobund-Wistar rat. *Prog. Clin. Biol. Res.* **287**, 241–246 (1989).
50. Richie, J. P. Jr et al. Methionine restriction increases blood glutathione and longevity in F344 rats. *FASEB J.* **8**, 1302–1307 (1994).
51. Bernardes de Jesus, B. et al. Telomerase gene therapy in adult and old mice delays aging and increases longevity without increasing cancer. *EMBO Mol. Med.* **4**, 691–704 (2012).
52. Okano, M., Bell, D. W., Haber, D. A. & Li, E. DNA methyltransferases Dnmt3a and Dnmt3b are essential for de novo methylation and mammalian development. *Cell* **99**, 247–257 (1999).
53. Childs, B. G., Durik, M., Baker, D. J. & van Deursen, J. M. Cellular senescence in aging and age-related disease: from mechanisms to therapy. *Nat. Med.* **21**, 1424–1435 (2015).
54. Conboy, I. M. & Rando, T. A. Heterochronic parabiosis for the study of the effects of aging on stem cells and their niches. *Cell Cycle* **11**, 2260–2267 (2012).
55. Yankova, T., Dubiley, T., Shytikov, D. & Pishel, I. Three month heterochronic parabiosis has a deleterious effect on the lifespan of young animals, without a positive effect for old animals. *Rejuvenation Res.* **25**, 191–199 (2022).
56. Castellano, J. M. et al. Human umbilical cord plasma proteins revitalize hippocampal function in aged mice. *Nature* **544**, 488–492 (2017).
57. Salpeter, S. J. et al. Systemic regulation of the age-related decline of pancreatic β-cell replication. *Diabetes* **62**, 2843–2848 (2013).
58. Villeda, S. A. et al. The ageing systemic milieu negatively regulates neurogenesis and cognitive function. *Nature* **477**, 90–94 (2011).
59. Rando, T. A. & Wyss-Coray, T. Asynchronous, contagious and digital aging. *Nat. Aging* **1**, 29–35 (2021).
60. Pálovics, R. et al. Molecular hallmarks of heterochronic parabiosis at single-cell resolution. *Nature* **603**, 309–314 (2022).
61. Conese, M., Carbone, A., Beccia, E. & Angiolillo, A. The fountain of youth: a tale of parabiosis, stem cells, and rejuvenation. *Open Med.* **12**, 376–383 (2017).
62. Elabd, C. et al. Oxytocin is an age-specific circulating hormone that is necessary for muscle maintenance and regeneration. *Nat. Commun.* **5**, 4082 (2014).
63. Stölzel, F. et al. Dynamics of epigenetic age following hematopoietic stem cell transplantation. *Haematologica* **102**, e321–e323 (2017).
64. Mehdipour, M. et al. Rejuvenation of three germ layers tissues by exchanging old blood plasma with saline-albumin. *Aging* **12**, 8790–8819 (2020).
65. Baht, G. S. et al. Meteorin-like facilitates skeletal muscle repair through a Stat3/IGF-1 mechanism. *Nat. Metab.* **2**, 278–289 (2020).
66. Krueger, F. & Andrews, S. R. Bismark: a flexible aligner and methylation caller for Bisulfite-Seq applications. *Bioinformatics* **27**, 1571–1572 (2011).
67. Dobin, A. et al. STAR: ultrafast universal RNA-seq aligner. *Bioinformatics* **29**, 15–21 (2013).
68. Liao, Y., Smyth, G. K. & Shi, W. featureCounts: an efficient general purpose program for assigning sequence reads to genomic features. *Bioinformatics* **30**, 923–930 (2014).
69. Love, M. I., Huber, W. & Anders, S. Moderated estimation of fold change and dispersion for RNA-seq data with DESeq2. *Genome Biol.* **15**, 550 (2014).
70. Robinson, M. D., McCarthy, D. J. & Smyth, G. K. edgeR: a Bioconductor package for differential expression analysis of digital gene expression data. *Bioinformatics* **26**, 139–140 (2010).
71. Benjamini, Y. & Hochberg, Y. Controlling the false discovery rate: a practical and powerful approach to multiple testing. *J. R. Stat. Soc. B* **57**, 289–300 (1995).
72. Anders, S. & Huber, W. Differential expression analysis for sequence count data. *Genome Biol.* **11**, R106 (2010).
73. Huffman, K. M. et al. Exercise protects against cardiac and skeletal muscle dysfunction in a mouse model of inflammatory arthritis. *J. Appl. Physiol.* **130**, 853–864 (2021).
74. White, J. P. et al. The AMPK/p27^{Kip1} axis regulates autophagy/apoptosis decisions in aged skeletal muscle stem cells. *Stem Cell Reports* **11**, 425–439 (2018).

Acknowledgements

J.P.W. was supported by National Institutes of Health (NIH) grant nos. K01AG056664 and R21AG065943. V.N.G. was supported by NIH grant nos. R01AG067782, P01AG047200 and R01AG065403. D.E.L. was supported by NIH training grant no. T32HL007057. S.H. acknowledges support from the Milky Way Research Foundation and the Epigenetic Clock Development Foundation, and A. Tyshkovskiy and S.E.D. acknowledge support from the Interdisciplinary Scientific and Educational School of Moscow University 'Molecular Technologies of the Living Systems and Synthetic Biology'. We thank the Duke Behavioral Core for support on this project. We also thank T. Fox for help with schematic figures. Figure icons were partially created with BioRender.com. The funders had no role in study design, data collection, data analysis, decision to publish, or preparation of the manuscript.

Author contributions

B.Z., D.E.L., V.N.G. and J.P.W. conceived the project. D.E.L., G.S.B., A.B., L.K.M. and J.P.W. carried out the animal experiments. A. Trapp, D.E.L. and B.Z. designed the figures. A. Trapp, A. Tyshkovskiy and B.Z. performed the gene expression analyses. B.Z., A. Trapp and C.K. conducted the DNA methylation clock analyses based on RRBS. B.Z., A. Trapp, A.T.L. and S.H. conducted the analyses based on the microarrays. A.V.S. contributed to the enrichment analyses. S.E.D. contributed to data interpretation. V.N.G. and J.P.W. supervised the project. B.Z., D.E.L., A. Trapp, V.N.G. and J.P.W. wrote the paper with final approval from all coauthors.

Competing interests

The authors declare no competing interests.

Additional information

Extended data is available for this paper at https://doi.org/10.1038/s43587-023-00451-9.

Supplementary information The online version contains supplementary material available at https://doi.org/10.1038/s43587-023-00451-9.

Correspondence and requests for materials should be addressed to Vadim N. Gladyshev or James P. White.

Peer review information *Nature Aging* thanks the anonymous reviewers for their contribution to the peer review of this work.

https://doi.org/10.1038/s43587-023-00451-9

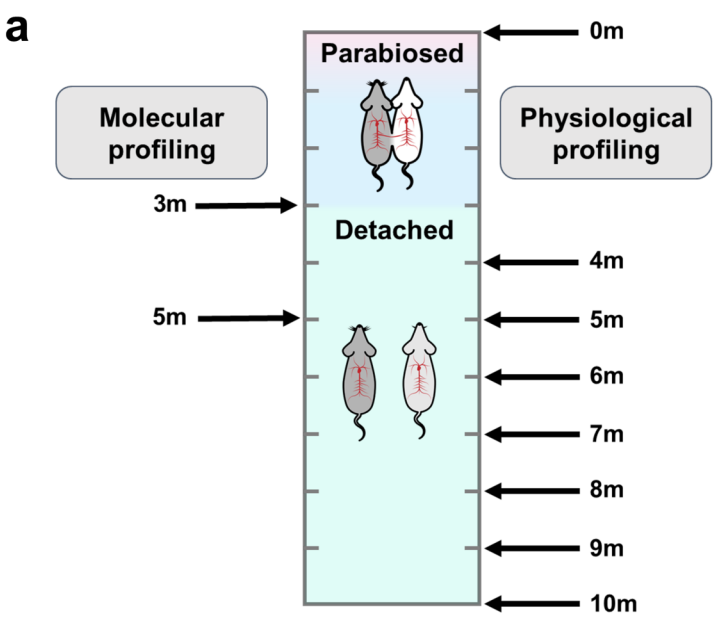

	Pairs attempted			Individual died during surgery			Individual died during detachment		
Experimental groups	Young ISO	Old ISO	HET	Young ISO	Old ISO	HET	Young ISO	Old ISO	HET
Physiological	5	8	15	0	4	4	0	2	1
Longevity		16	25		6	3		3	2
Omics	4	5	8	2	2	2	0	1	0

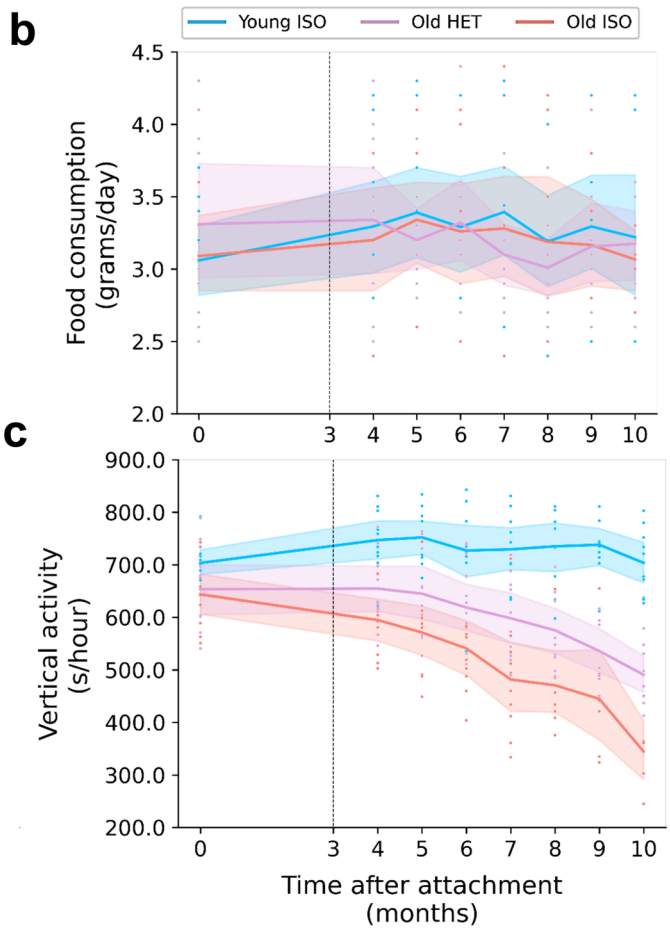

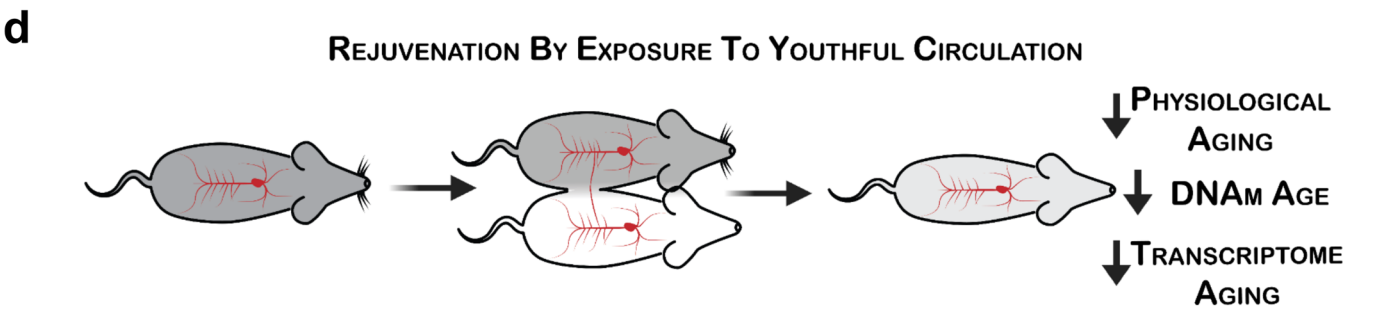

Extended Data Fig. 1 | Timeline of molecular and physiological profiling. **a**, Schematic timeline of the molecular (transcriptomic & epigenetic) and physiological profiling presented in this study (top) as well as a table (bottom) highlighting mortality rates at various parts in the parabiosis protocol (numbers represent individual mice, not pairs). Samples were taken immediately after the parabiosis period (month 3), or after a 2-month detachment period (month 5). Physiological profiling was performed before the parabiosis experiment (month 0), and then every month from month 4 to month 10. Data in the table (bottom) is separated by experimental purposes and ages of the pairs. Mortality rate across experiments for each group: Young ISO: 11% mortality during PB, 0% during detach; Old ISO: 20% mortality during PB, 13% during detach. Old HET: 19% mortality during PB, 7% during detach. **b**, Changes in food consumption resulting from parabiosis. Lines depict mean changes with 95% confidence intervals. Individual observations are shown as points. Young isochronic (Young ISO) mice are shown in blue, old heterochronic (Old HET) mice are shown in purple, and old isochronic (Old ISO) mice are shown in red. Dashed line depicts time of detachment. **c**, Changes in vertical activity resulting from parabiosis. Lines depict mean changes with 95% confidence intervals. Individual observations are shown as points. Legend is the same as (**b**). **d**, Schematic of the experimental workflow and associated findings.

https://doi.org/10.1038/s43587-023-00451-9

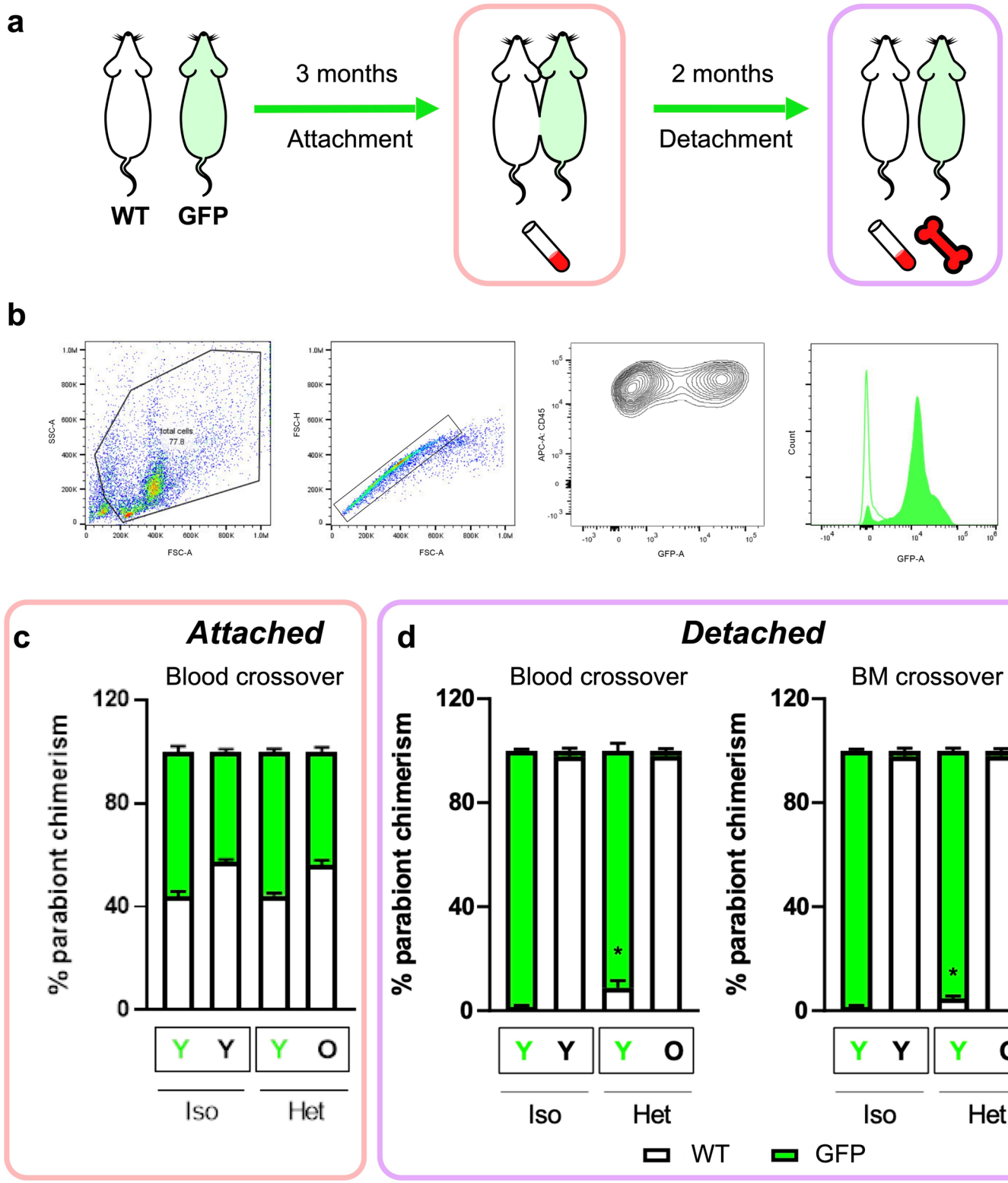

Extended Data Fig. 2 | Blood mixture analyses after 3 months of parabiosis. **a**, Schematic of experiments to analyze the blood chimerism after attachment and detachment. Green represents GFP (+) mice, white represents wild-type mice. **b**, Gating scheme applied to all downstream blood analysis between GFP and wild-type mice. Cells were ultimately gated on GFP (+) (x-axis) and CD45-APC (+) (y-axis). **c**, Percentage of blood crossover during attachment. **d**, Percentage of blood (left) and bone marrow (BM, right) crossover after 2-month detachment, calculated as the % GFP (+) and (-) cells, $n = 3$ biological replicates group. Bars represent mean +/− SEM of cell proportions labelled GFP+ and GFP-(WT).

https://doi.org/10.1038/s43587-023-00451-9

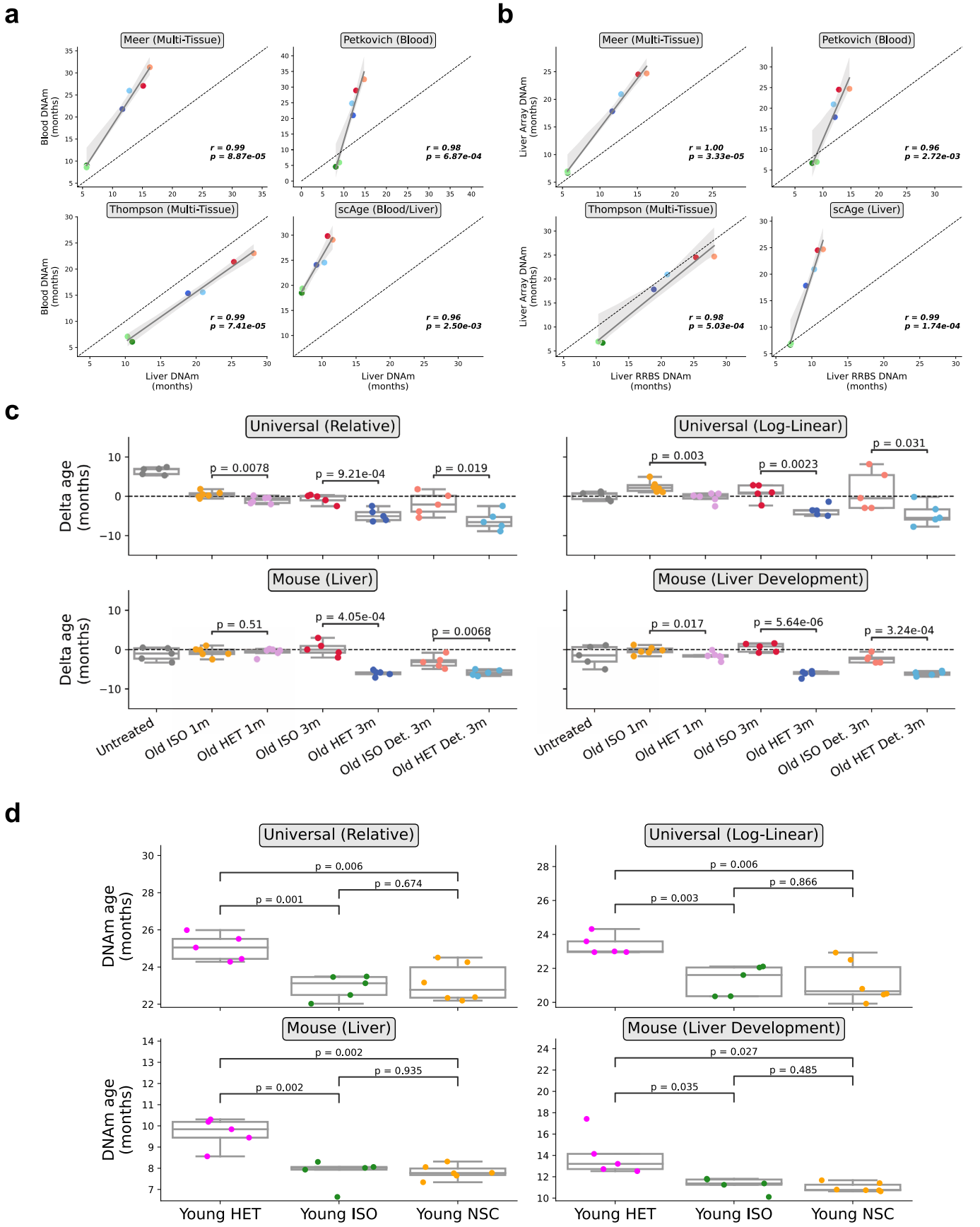

Extended Data Fig. 3 | See next page for caption.

https://doi.org/10.1038/s43587-023-00451-9

Extended Data Fig. 3 | Relationship of DNAm age across tissues and platforms, delta age analysis, and effect of surgery. a, Scatterplots highlighting the association of liver and blood DNAm predictions based on RRBS sequencing across 6 different group: young isochronic (Young ISO), young isochronic detached (Young ISO Det.), old heterochronic (Old HET), old isochronic (Old ISO), old heterochronic detached (Old HET Det.), and old isochronic detached (Old ISO Det.). Each point depicts the mean DNAm prediction for a particular tissue for that group. The clock used for predictions is shown in the top part of each panel. The Pearson correlation *(r)* is shown in each panel, along with its associated two-tailed *P* value. Linear regression lines (dark grey) with 95% confidence intervals (light grey) are shown. **b**, Scatterplots highlighting the association of liver DNAm predictions based on RRBS sequencing and methylation array profiling across 6 different groups (same legend as **a**). The clock used for RRBS predictions is shown in the top part of each panel. The mouse liver development clock was used for array predictions given that it showed the greatest changes in epigenetic age comparing long-term old heterochronic and isochronic mice. **c**, Delta age (epigenetic age minus chronological age) of liver samples from old heterochronic mice, old isochronic controls and untreated controls based on universal relative age mammalian, universal log-linear transformed age mammalian, liver, and development liver clocks. Dashed line denotes a delta age of 0 (epigenetic age = chronological age). Points above this line depict age acceleration (epigenetic age > chronological age), while points below this line depict age deceleration (epigenetic age < chronological age). $n = 5$ per group. **d**, Epigenetic age of liver samples from 8-month old non-surgical control mice (Young NSC), isochronic detached (Young ISO) and heterochronic detached mice (Young HET), based on the universal relative age mammalian, universal log-linear transformed age mammalian, liver, and liver development clocks. $n = 5$ per group for parabiosed mice and 6 per group for controls. Box plots represent 25–75 percentile and 1.5x IQR. Two-tailed Welch's t-tests were used for statistical analyses.

https://doi.org/10.1038/s43587-023-00451-9

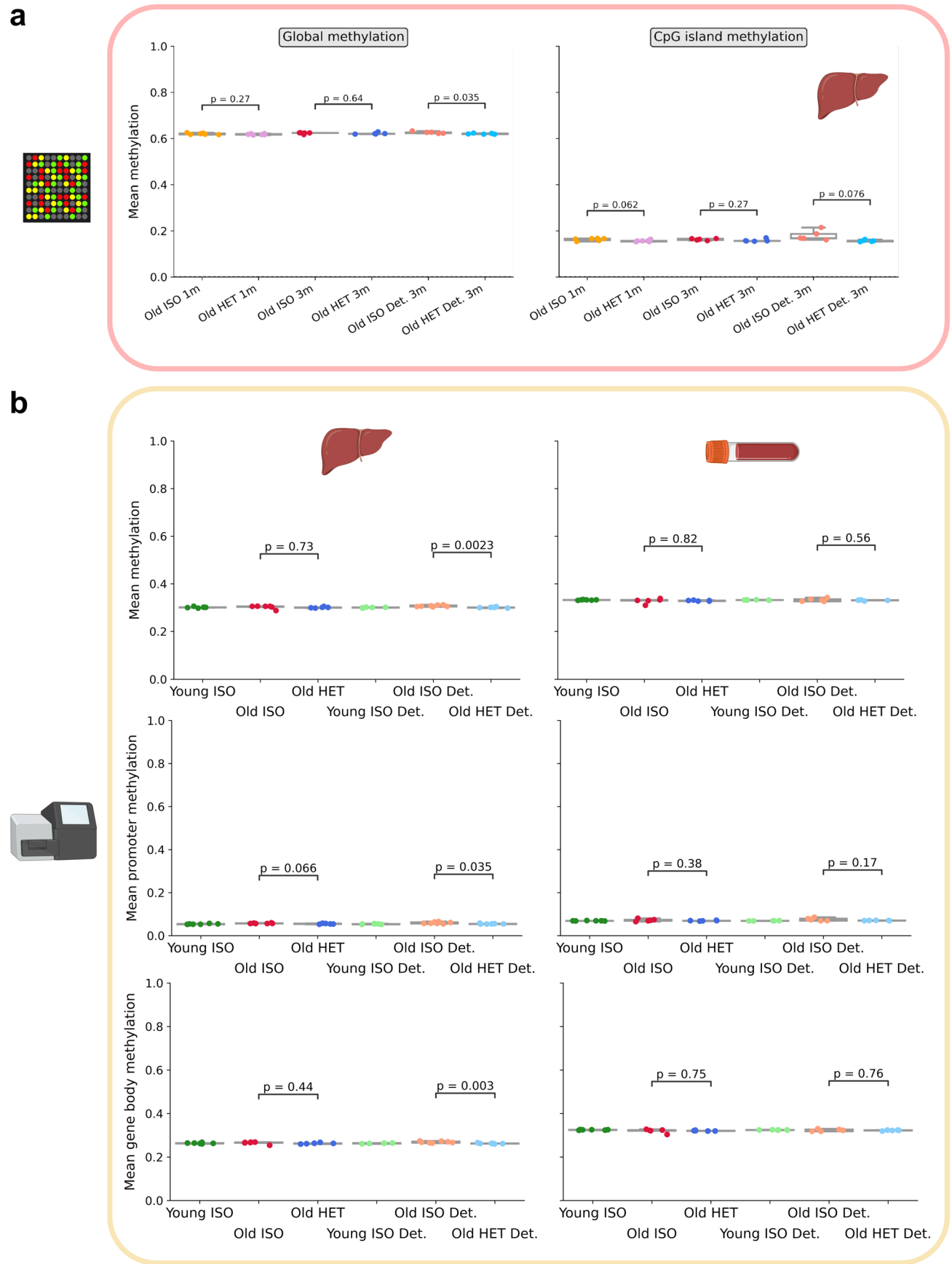

Extended Data Fig. 4 | See next page for caption.

https://doi.org/10.1038/s43587-023-00451-9

Extended Data Fig. 4 | Mean methylation in array and RRBS methylation profiles. a, Mean liver methylation assayed by the Mammalian Methylation Array (HorvathMammalMethylChip40), both based on all sites in the array (left) and only sites in CpG islands (right). $n = 5$ samples per group. **b**, Mean global methylation (top), promoter methylation (middle), and gene body methylation (bottom) of liver (left) and blood (right) RRBS samples. Mean methylation was assayed across 1,014,243 CpGs (top), 11,842 promoters (middle), and 13,811 gene bodies (bottom). $n = 4$ samples per group. Box plots represent 25–75 percentile and 1.5x IQR. Two-tailed Welch's t-test were used for statistical analysis. Schematic tissues in each panel indicate the source of the sample.

https://doi.org/10.1038/s43587-023-00451-9

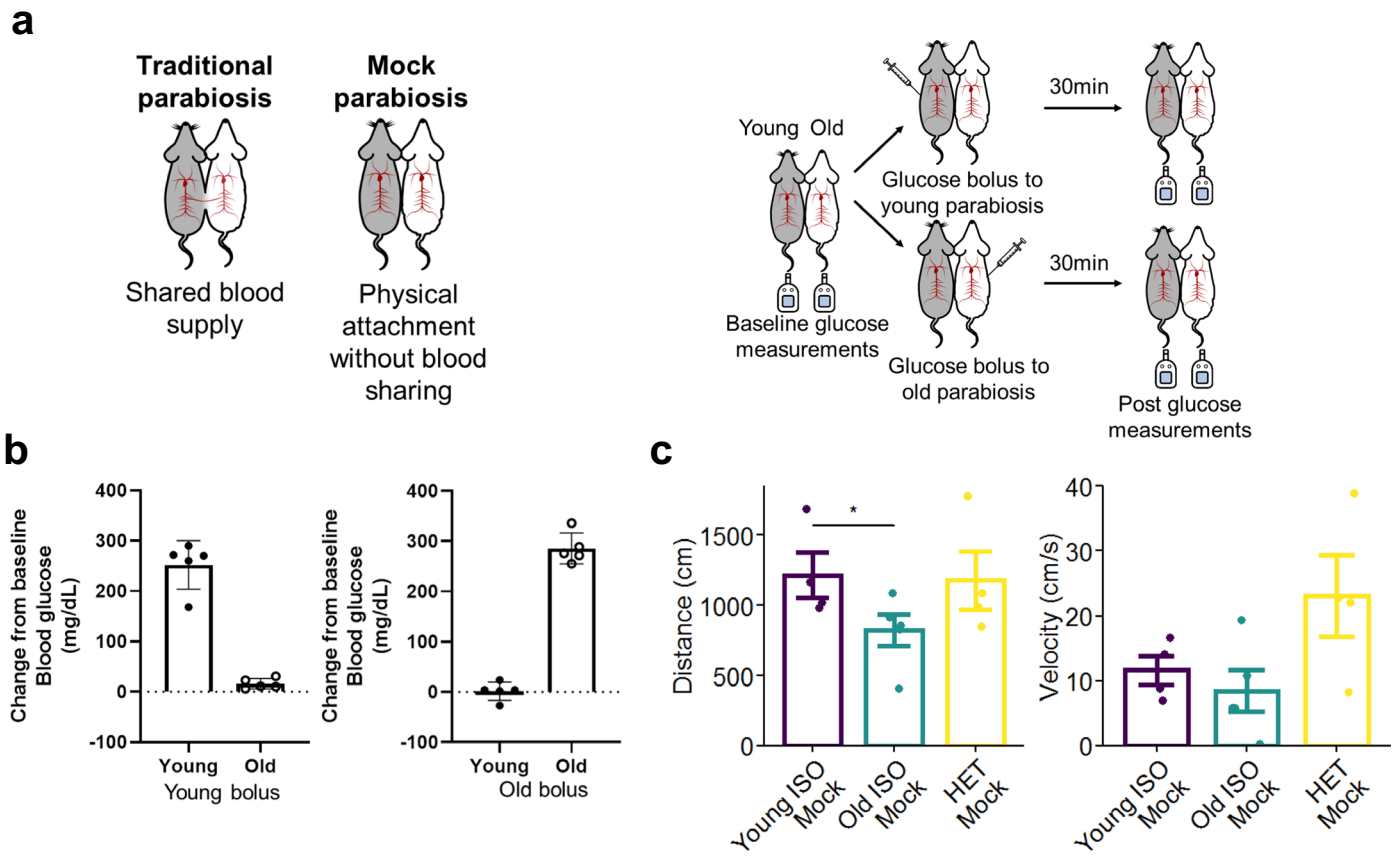

Extended Data Fig. 5 | Physiological tests of a mock parabiosis procedure to assess the interaction of parabiosis and exercise. a, Schematic of the experiment to test blood sharing using glucose levels. Glucose is injected into one mouse and subsequently assessed in both mice in mock parabiosis pairs. **b**, Blood glucose level changes in pairs starting with a young (left) and old (right) glucose bolus to determine blood sharing; $n = 5$ biological replicates/group. No statistical test was performed. **c**, Moving distance in cm (left), and velocity (right) in the old isochronic, young isochronic and heterochronic mock parabiosis pairs. $n = 4$ biological replicates/ group. Bars represents mean +/− SEM. $P_{distance}$(Young ISO−Old ISO) = 0.034 calculated by two-tailed, Student's t-test. **d**, Movement tracking in the old isochronic, young isochronic and heterochronic mock parabiosis pairs.

https://doi.org/10.1038/s43587-023-00451-9

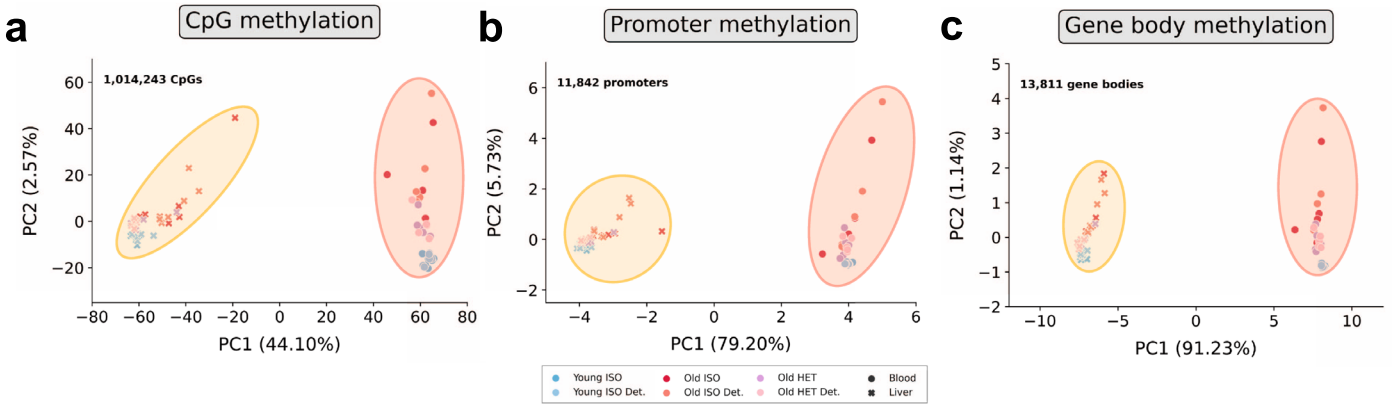

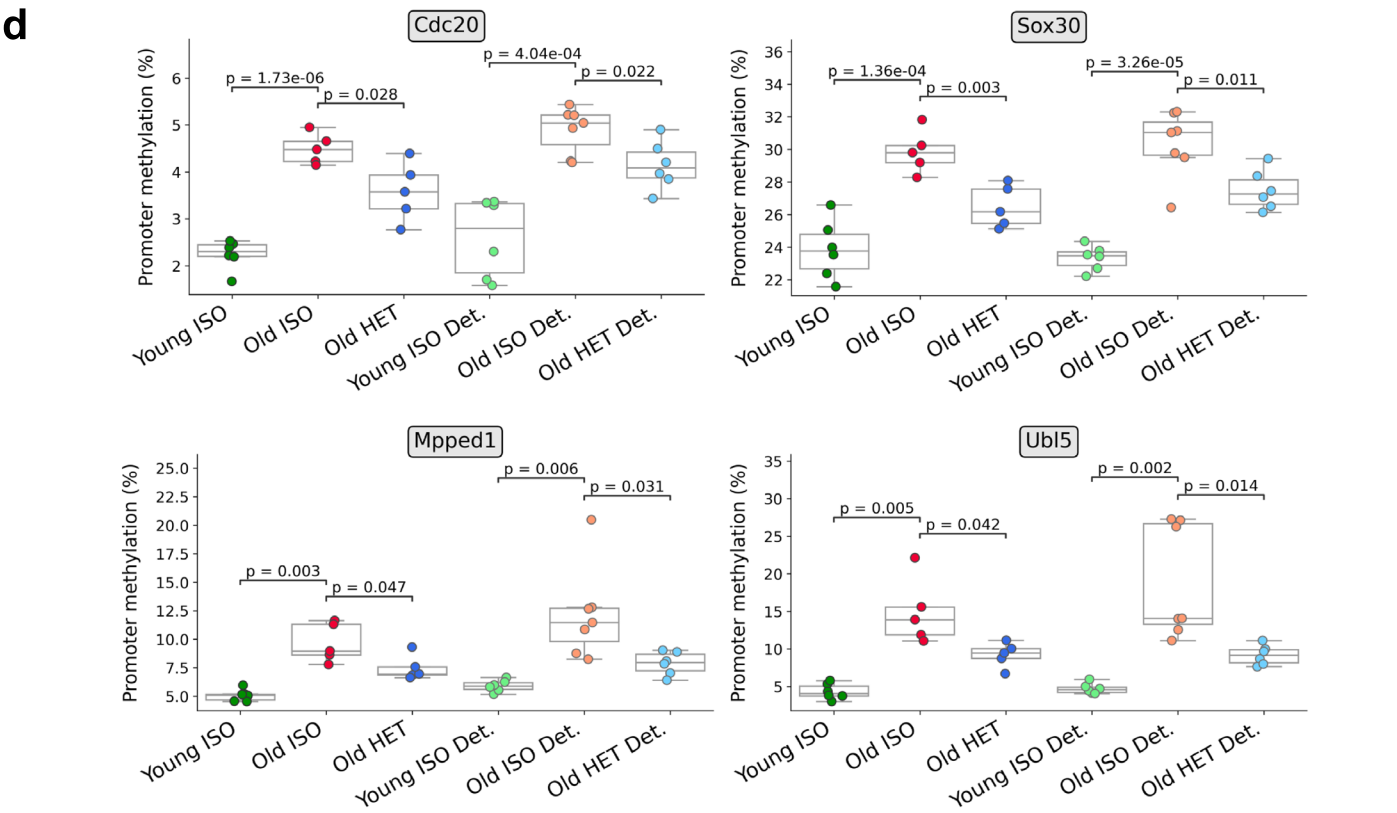

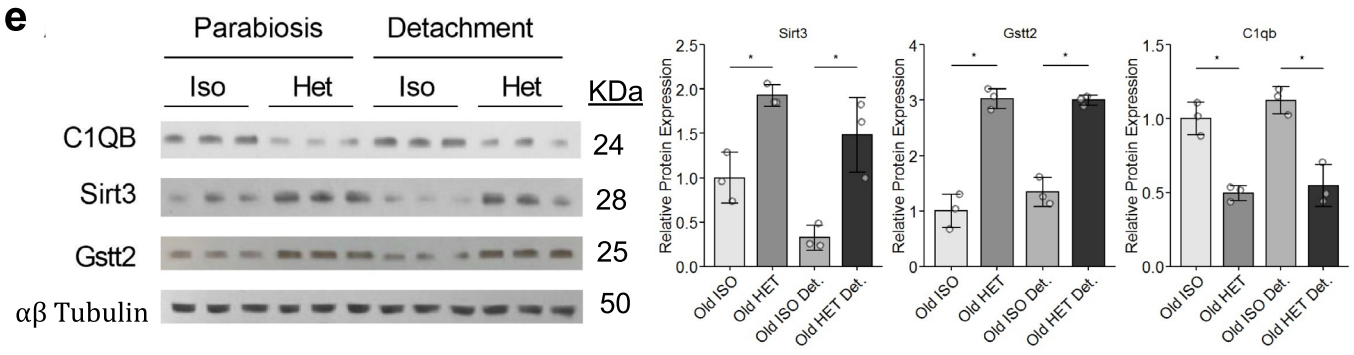

Extended Data Fig. 6 | See next page for caption.

https://doi.org/10.1038/s43587-023-00451-9

Extended Data Fig. 6 | Tissue specificity of RRBS epigenomic profiles, promoter methylation changes, and proteomic dynamics in HPB. **a-c**, Principal component analysis (PCA) of CpG methylation across 1,014,243 CpG sites **(a)**, 11,842 promoters **(b)**, and 13,811 gene bodies **(c)** in $n = 36$ liver samples and $n = 32$ blood samples, with 6 different groups in both tissues: young isochronic (Young ISO), young isochronic detached (Young ISO Det.), old heterochronic (Old HET), old isochronic (Old ISO), old heterochronic detached (Old HET Det.), and old isochronic detached (Old ISO Det.). In all the PCA plots, tissue of origin is the largest source of variation (44–91%). **d**, Promoter methylation of *Cdc20*, *Sox30*, *Mpped1*, and *Ubl5* across liver RRBS samples. Genes were identified after passing a significance threshold ($p < 0.05$) when comparing young and old mice, as well as old heterochronic and isochronic mice in both attached and detached groups. $n = 6$ biological replicates/group. *P* value's calculated by two-tailed Welch's t-tests. Box plots represent Mean, 25–75 quartiles and 1.5x IQR. **e**, Western blot validation (left) and relative protein expression quantification (right) of *Sirt3*, *Gstt2* and *C1qb* in mice subjected to parabiosis.

https://doi.org/10.1038/s43587-023-00451-9

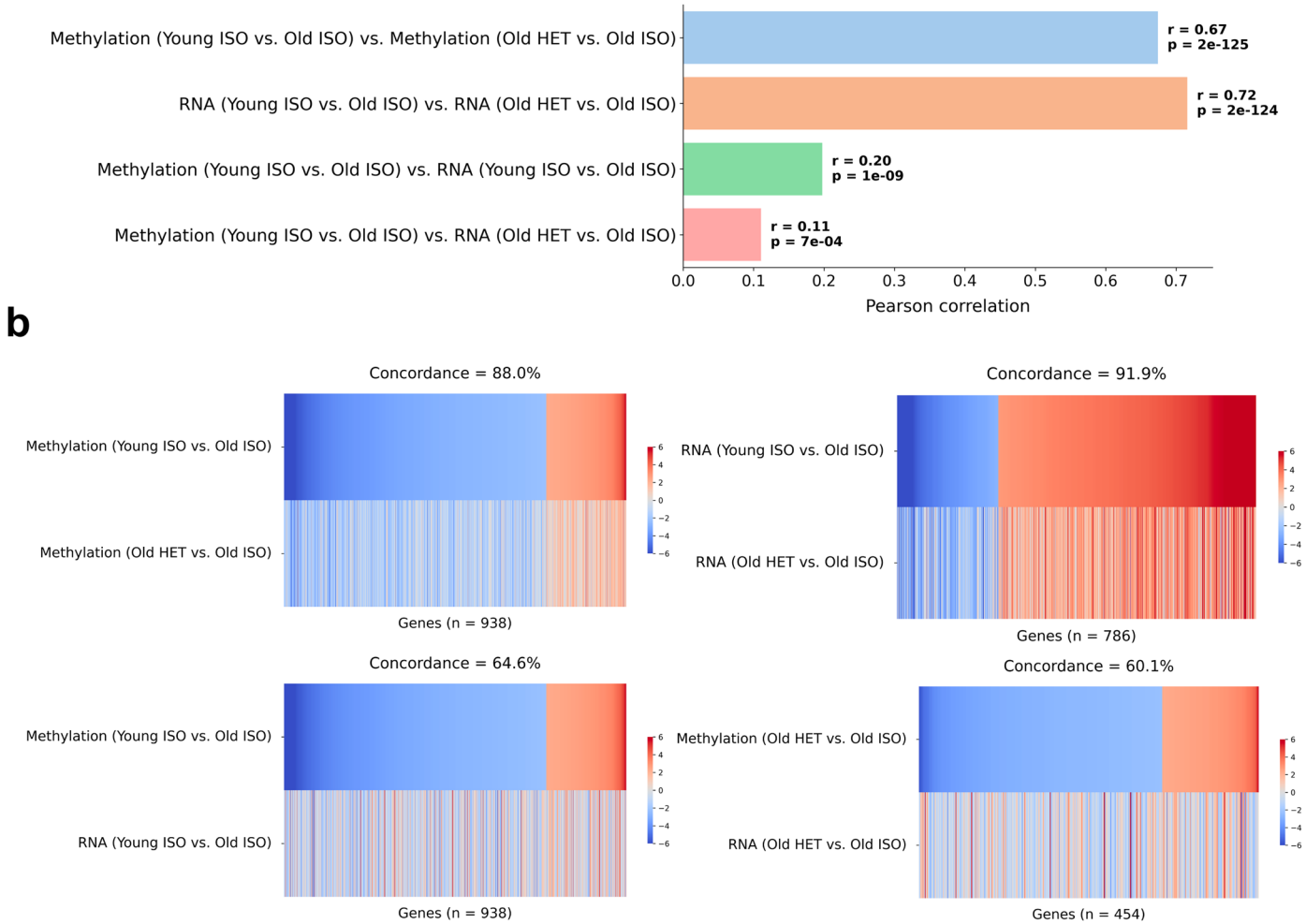

Extended Data Fig. 7 | Interactions between different omics modalities. **a**, Correlation of changes across experimental groups and readout types. For each comparison in parentheses (that is Young ISO vs. Old ISO), a z-score was computed for either promoter methylation or gene expression. The Pearson correlation of these z-scores was then determined for genes passing a differential expression/methylation threshold of $p < 0.05$ for the first (left) group listed in each comparison. **b**, Heat maps highlighting the concordance of readouts and experimental groups. For each heat map, the z-score of genes that are significantly ($p < 0.05$) differentially expressed or methylated is shown. Genes are ordered by the z-score in the top group. Color bar on the right denotes z-score. The directional concordance, a measure of how directionally aligned the changes between the two readouts/groups are, is shown at the top of each heat map. 50% concordance represents random changes across groups Two-tailed Benchamini-Hochberg corrected FDR was calculated to compare groups.

https://doi.org/10.1038/s43587-023-00451-9

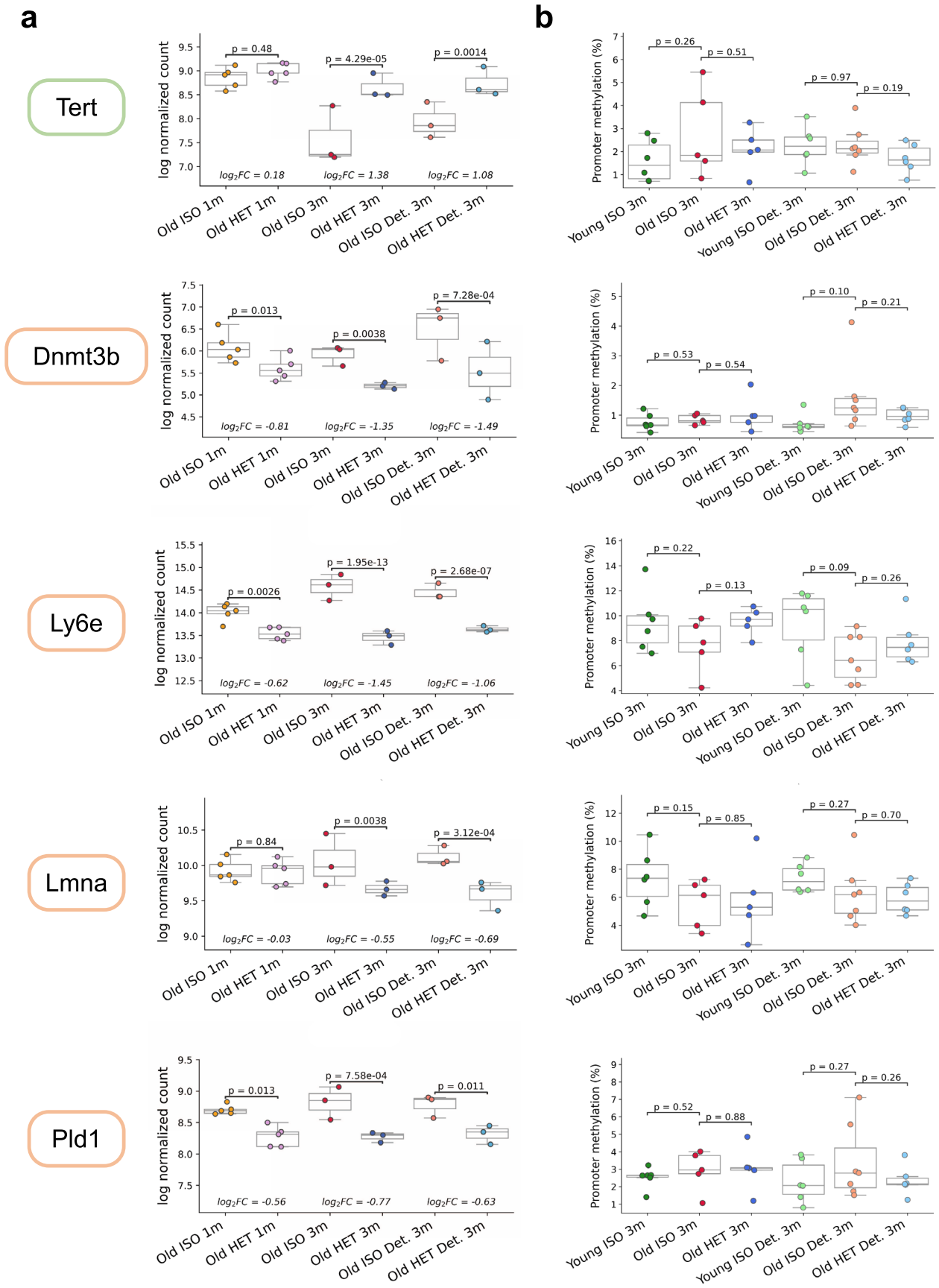

Extended Data Fig. 8 | See next page for caption.

https://doi.org/10.1038/s43587-023-00451-9

Extended Data Fig. 8 | Transcriptomic and epigenetic changes resulting from HPB. a, Boxplots of RLD-transformed, log-normalized counts of *Tert*, *Dnmt3b*, *Ly6e*, *Lmna and Pld1* across 6 groups (from left to right: old short-term isochronic ($n = 5$), old short-term heterochronic ($n = 5$), old long-term isochronic ($n = 3$), old long-term heterochronic ($n = 3$), old long-term isochronic detached ($n = 3$), and old long-term heterochronic detached ($n = 3$). **b**, Mean promoter methylation of the genes mentioned in **(a)** across liver RRBS samples across 6 groups (from left to right: young long-term isochronic ($n = 6$), old long-term isochronic ($n = 5$), old long-term heterochronic ($n = 5$), young long-term isochronic detached ($n = 6$), old long-term isochronic detached ($n = 7$), and old long-term heterochronic detached ($n = 6$). Color of the box around each gene signifies directionality (green: gene expression increases in Old HET mice compared to ISO, orange: gene expression decreases in Old HET mice compared to ISO). Despite evident changes in expression patterns for these genes, no significant changes in promoter methylation are observed. N represents biological replicates for each group. *P* values determined by two-tailed Welch's t-test. Box plots represent median, 25–75 percentile and 1.5x IQR.

https://doi.org/10.1038/s43587-023-00451-9

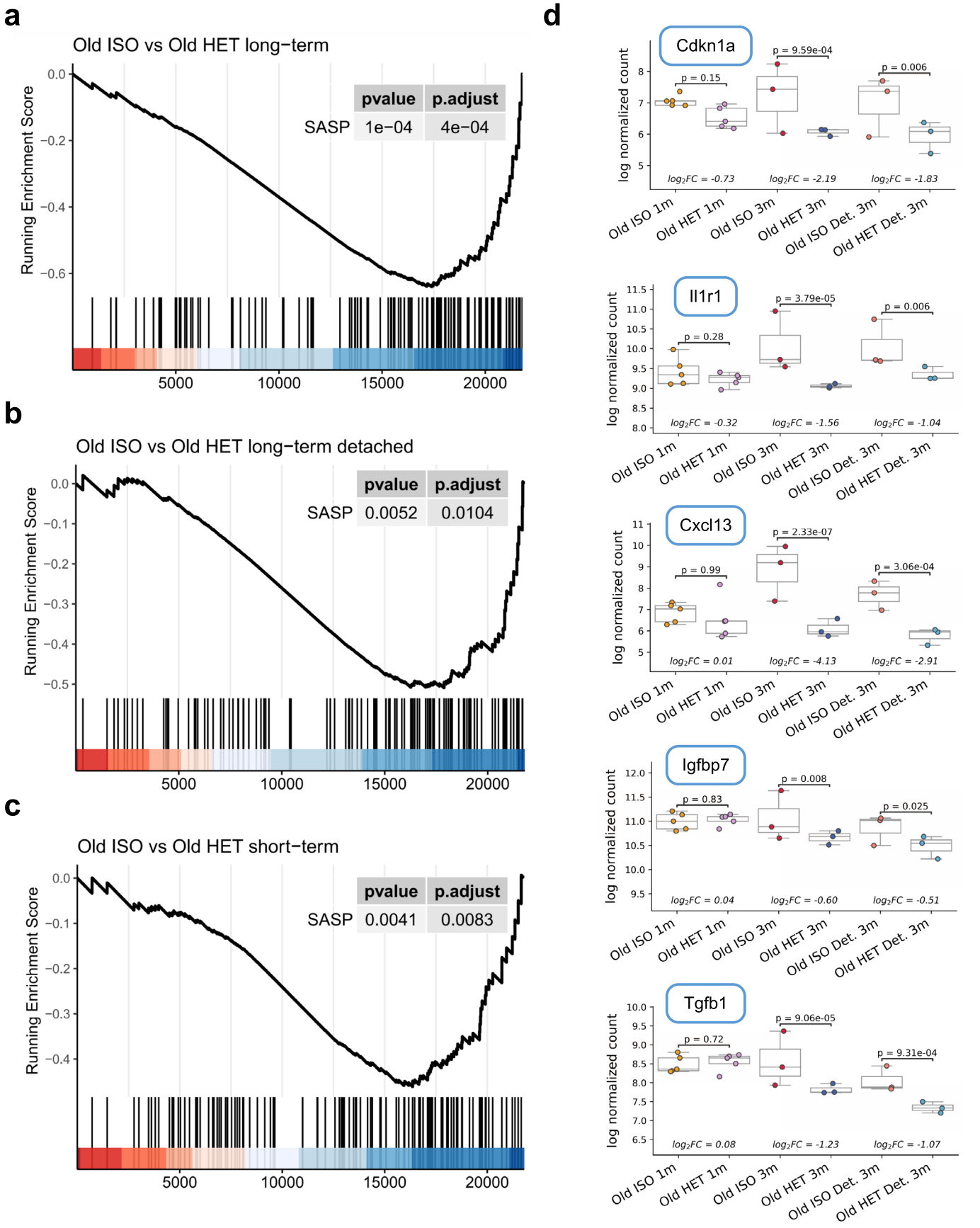

Extended Data Fig. 9 | See next page for caption.

https://doi.org/10.1038/s43587-023-00451-9

Extended Data Fig. 9 | SASP enrichment and differential expression across long-term and short-term HPB. a-c, Running enrichment score for the senescence-associated secretory phenotype (SASP) gene set, comparing in **(a)** old isochronic and old heterochronic mice from the long-term HPB, in **(b)** old detached isochronic and old detached heterochronic mice from long-term HPB, and in **(c)** old detached isochronic and old detached heterochronic mice from short-term HPB. The *P* values for the gene set enrichment, along with the adjusted *P* value are shown in each panel. Positions of individual genes in the gene set are shown as black bars near the bottom of each panel. Long-term attached HPB shows the greatest negative enrichment for heterochronic samples, followed by detached long-term HPB and attached short-term HPB, respectively. **d**, Boxplots of RLD-transformed, log-normalized count of five SASP genes across 6 groups (from left to right: old short-term isochronic ($n = 5$), old short-term heterochronic ($n = 5$), old long-term isochronic ($n = 3$), old long-term heterochronic ($n = 3$), old long-term isochronic detached ($n = 3$), and old long-term heterochronic detached ($n = 3$). The $\log_2$ fold-change ($\log_2$FC) and associated *P* value are shown as calculated by two-tailed Welch's test. Box plots represent median, 25–75 percentile and 1.5x IQR.

https://doi.org/10.1038/s43587-023-00451-9

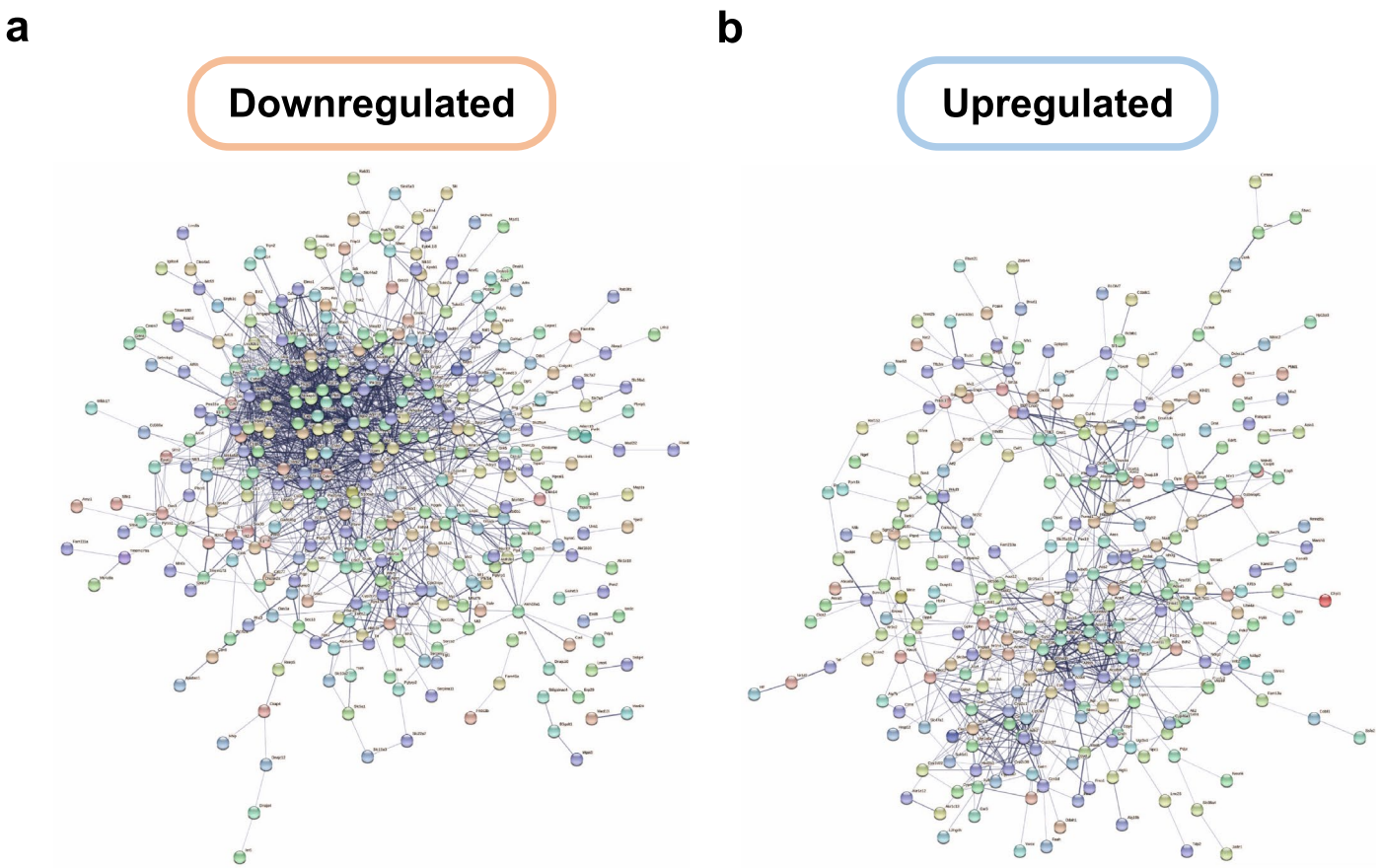

Extended Data Fig. 10 | STRING network representation of significantly down- and upregulated genes. a, STRING network representation of significantly downregulated genes in livers of old heterochronic mice (n = 421 genes) compared to isochronic mice immediately after detachment or after a 2-month detachment period (protein-protein interaction q value < 1e-16). Genes were filtered based on directionality and absolute value of the $\log_2$FC.

b, STRING network representation of significantly upregulated genes in livers of old heterochronic mice (n = 337 genes) compared to isochronic mice immediately after detachment or after a 2-month detachment period (protein-protein interaction q value < 1e-16). Genes were filtered based on directionality and absolute value of the $\log_2$FC.

nature portfolio

Corresponding author(s): James White, Vadim Gladyshev

Last updated by author(s): Feb 21, 2023

Reporting Summary

Nature Portfolio wishes to improve the reproducibility of the work that we publish. This form provides structure for consistency and transparency in reporting. For further information on Nature Portfolio policies, see our Editorial Policies and the Editorial Policy Checklist.

Statistics

For all statistical analyses, confirm that the following items are present in the figure legend, table legend, main text, or Methods section.

n/a	Confirmed
☐	☒ The exact sample size (*n*) for each experimental group/condition, given as a discrete number and unit of measurement
☐	☒ A statement on whether measurements were taken from distinct samples or whether the same sample was measured repeatedly
☐	☒ The statistical test(s) used AND whether they are one- or two-sided *Only common tests should be described solely by name; describe more complex techniques in the Methods section.*
☐	☒ A description of all covariates tested
☐	☒ A description of any assumptions or corrections, such as tests of normality and adjustment for multiple comparisons
☐	☒ A full description of the statistical parameters including central tendency (e.g. means) or other basic estimates (e.g. regression coefficient) AND variation (e.g. standard deviation) or associated estimates of uncertainty (e.g. confidence intervals)
☐	☒ For null hypothesis testing, the test statistic (e.g. *F*, *t*, *r*) with confidence intervals, effect sizes, degrees of freedom and *P* value noted *Give P values as exact values whenever suitable.*
☒	☐ For Bayesian analysis, information on the choice of priors and Markov chain Monte Carlo settings
☒	☐ For hierarchical and complex designs, identification of the appropriate level for tests and full reporting of outcomes
☐	☒ Estimates of effect sizes (e.g. Cohen's *d*, Pearson's *r*), indicating how they were calculated

Our web collection on statistics for biologists contains articles on many of the points above.

Software and code

Policy information about availability of computer code

Data collection	*Provide a description of all commercial, open source and custom code used to collect the data in this study, specifying the version used OR state that no software was used.*
Data analysis	There was script for ScAge clock analysis, which is available at https://github.com/alex-trapp/scage. Both R and Python were used to analyze data

For manuscripts utilizing custom algorithms or software that are central to the research but not yet described in published literature, software must be made available to editors and reviewers. We strongly encourage code deposition in a community repository (e.g. GitHub). See the Nature Portfolio guidelines for submitting code & software for further information.

Data

Policy information about availability of data

All manuscripts must include a data availability statement. This statement should provide the following information, where applicable:

- Accession codes, unique identifiers, or web links for publicly available datasets
- A description of any restrictions on data availability
- For clinical datasets or third party data, please ensure that the statement adheres to our policy

Data Availability: The data obtained in this study will be deposited to GEO with the accession number GSE224447.

Field-specific reporting

Please select the one below that is the best fit for your research. If you are not sure, read the appropriate sections before making your selection.

☒ Life sciences ☐ Behavioural & social sciences ☐ Ecological, evolutionary & environmental sciences

For a reference copy of the document with all sections, see nature.com/documents/nr-reporting-summary-flat.pdf

Life sciences study design

All studies must disclose on these points even when the disclosure is negative.

Sample size	For the physiological experiments, sample sizes were based on previous experience in the White lab (Huffman, JAP. 2021). For both transcriptomics and epigenetics analysis, sample sizes were based on previous experience in the Gladyshev lab (Petkovich, Cell Met. 2017).
Data exclusions	According to our PCA analyses, two blood samples and one liver sample that were evident outliers were removed from downstream epigenetic aging analyses. This is included in the methods section in "Application of mouse epigenetic clocks to RRBS datasets". *removal of these data points did not affect the outcome of any statistical analysis.
Replication	Phenotypical responses (body mass, body composition, and voluntary movement distance) to HPB were examined in two independent experiments. Results were reproducible between experiments.
Randomization	Mice were randomized into either heterochronic or isochronic treatments.
Blinding	Physiological experiments performed post-detachment were blinded for parabiosis groups. However, due to obvious aging phenotypes, blinding was difficult for the young vs old groups.

Reporting for specific materials, systems and methods

We require information from authors about some types of materials, experimental systems and methods used in many studies. Here, indicate whether each material, system or method listed is relevant to your study. If you are not sure if a list item applies to your research, read the appropriate section before selecting a response.

Materials & experimental systems

n/a	Involved in the study
☒	☐ Antibodies
☒	☐ Eukaryotic cell lines
☒	☐ Palaeontology and archaeology
☐	☒ Animals and other organisms
☒	☐ Human research participants
☒	☐ Clinical data
☒	☐ Dual use research of concern

Methods

n/a	Involved in the study
☒	☐ ChIP-seq
☐	☒ Flow cytometry
☒	☐ MRI-based neuroimaging

Animals and other organisms

Policy information about studies involving animals; ARRIVE guidelines recommended for reporting animal research

Laboratory animals	We have reported information about laboratory animals, including gender, age and strain in the MATERIALS AND METHODS/Mouse models section
Wild animals	*Provide details on animals observed in or captured in the field; report species, sex and age where possible. Describe how animals were caught and transported and what happened to captive animals after the study (if killed, explain why and describe method; if released, say where and when) OR state that the study did not involve wild animals.*
Field-collected samples	*For laboratory work with field-collected samples, describe all relevant parameters such as housing, maintenance, temperature, photoperiod and end-of-experiment protocol OR state that the study did not involve samples collected from the field.*
Ethics oversight	*Identify the organization(s) that approved or provided guidance on the study protocol, OR state that no ethical approval or guidance was required and explain why not.*

Note that full information on the approval of the study protocol must also be provided in the manuscript.

Flow Cytometry

Plots

Confirm that:

☒ The axis labels state the marker and fluorochrome used (e.g. CD4-FITC).

☒ The axis scales are clearly visible. Include numbers along axes only for bottom left plot of group (a 'group' is an analysis of identical markers).

☒ All plots are contour plots with outliers or pseudocolor plots.

☒ A numerical value for number of cells or percentage (with statistics) is provided.

Methodology

Sample preparation	whole blood and bone marrow were analyzed for CD45(+) and GFP(+) immune cells
Instrument	Cell counts were performed on the Thermo Fisher Attune® NxT Acoustic Focusing Cytometer
Software	final analysis was performed with FloJo Software
Cell population abundance	Cell populations were calculated by percentage of total CD45 cells that were GFP(+)
Gating strategy	Cell were gated on CD45 (APC) and GFP

☒ Tick this box to confirm that a figure exemplifying the gating strategy is provided in the Supplementary Information.